



# Identification of psychiatric disorder subtypes from functional connectivity patterns in resting-state electroencephalography

Yu Zhang <sup>1,2,3,19</sup>, Wei Wu <sup>1,2,4,5,19</sup>, Russell T. Toll <sup>6</sup>, Sharon Naparstek <sup>1,2</sup>, Adi Maron-Katz <sup>1,2</sup>, Mallissa Watts <sup>1,2</sup>, Joseph Gordon <sup>1,2,5</sup>, Jisoo Jeong <sup>1,2</sup>, Laura Astolfi <sup>7,8</sup>, Emmanuel Shpigel <sup>1,2</sup>, Parker Longwell <sup>1,2</sup>, Kamron Sarhadi <sup>1,2</sup>, Dawlat El-Said <sup>1,2</sup>, Yuanqing Li <sup>4,9</sup>, Crystal Cooper <sup>6</sup>, Cherise Chin-Fatt <sup>6</sup>, Martijn Arns <sup>10,11,12,13</sup>, Madeleine S. Goodkind <sup>14</sup>, Madhukar H. Trivedi <sup>6,15</sup>, Charles R. Marmar <sup>16,17,18</sup> and Amit Etkin <sup>1,2,5</sup>

The understanding and treatment of psychiatric disorders, which are known to be neurobiologically and clinically heterogeneous, could benefit from the data-driven identification of disease subtypes. Here, we report the identification of two clinically relevant subtypes of post-traumatic stress disorder (PTSD) and major depressive disorder (MDD) on the basis of robust and distinct functional connectivity patterns, prominently within the frontoparietal control network and the default mode network. We identified the disease subtypes by analysing, via unsupervised and supervised machine learning, the power-envelope-based connectivity of signals reconstructed from high-density resting-state electroencephalography in four datasets of patients with PTSD and MDD, and show that the subtypes are transferable across independent datasets recorded under different conditions. The subtype whose functional connectivity differed most from those of healthy controls was less responsive to psychotherapy treatment for PTSD and failed to respond to an antidepressant medication for MDD. By contrast, both subtypes responded equally well to two different forms of repetitive transcranial magnetic stimulation therapy for MDD. Our data-driven approach may constitute a generalizable solution for connectome-based diagnosis.

Psychiatric diagnoses are defined based on constellations of symptoms that seek to characterize a particular condition with respect to both healthy individuals and other diagnoses. For example, post-traumatic stress disorder (PTSD) involves a range of emotional, cognitive and somatic symptoms that can develop after a person has experienced or witnessed a traumatic event in which serious harm to the individual occurred or was threatened<sup>1</sup>. Likewise, major depressive disorder (MDD) is characterized by sustained negative mood, often associated with biological, psychological or social sources of stress<sup>2</sup>. The traditional approach for studying the neurobiology of psychiatric conditions has followed this diagnostic framework through case–control studies whereby all patients with a given diagnosis are compared with healthy individuals. However, this approach has failed to deliver on hoped-for biomarkers due to high biological heterogeneity among patients with the same diagnosis and among healthy controls<sup>3–6</sup>. More importantly, such biological heterogeneity has substantial effects on treatment outcome, even

while often being independent of pre-treatment clinical symptoms. For example, while antidepressants have only modest superiority over placebo, this is in part because the clinical diagnosis of MDD encompasses biologically heterogeneous conditions that relate differentially to treatment outcome<sup>7–9</sup>. Likewise, even though psychotherapy is at present the most effective treatment for PTSD<sup>10</sup>, many patients are nonetheless non-responsive and display differences in brain function relative to responsive patients<sup>8,11</sup>. In neither case, however, are neurobiological differences related to clinical features, supporting the potential unique value of neurobiology in defining clinically relevant ‘disease subtypes’. These subtypes may furthermore exist within or between traditional psychiatric diagnoses<sup>12–16</sup>.

Most of the existing neuroimaging studies investigating disease subtypes, however, have used functional magnetic resonance imaging (fMRI)<sup>17–19</sup>, an important neuroimaging technology for studying the functional pathophysiology of brain disorders. Despite its popularity and success in early proof-of-concept subtyping efforts,

<sup>1</sup>Department of Psychiatry and Behavioral Sciences, Stanford University, Stanford, CA, USA. <sup>2</sup>Wu Tsai Neurosciences Institute, Stanford University, Stanford, CA, USA. <sup>3</sup>Department of Bioengineering, Lehigh University, Bethlehem, PA, USA. <sup>4</sup>School of Automation Science and Engineering, South China University of Technology, Guangzhou, China. <sup>5</sup>Alto Neuroscience, Inc., Los Altos, CA, USA. <sup>6</sup>Department of Psychiatry, Center for Depression Research and Clinical Care, Peter O’Donnell Jr. Brain Institute, UT Southwestern Medical Center, Dallas, TX, USA. <sup>7</sup>Department of Computer, Control and Management Engineering “Antonio Ruberti”, University of Rome Sapienza, Rome, Italy. <sup>8</sup>IRCCF Fondazione Santa Lucia, Rome, Italy. <sup>9</sup>Pazhou Lab, Guangzhou, China. <sup>10</sup>Research Institute Brainclinics, Brainclinics Foundation, Nijmegen, The Netherlands. <sup>11</sup>neuroCare Group, Munich, Germany. <sup>12</sup>Amsterdam UMC, University of Amsterdam, Department of Psychiatry, Location AMC, Amsterdam Neuroscience, Amsterdam, The Netherlands. <sup>13</sup>Department of Cognitive Neuroscience, Faculty of Psychology and Neuroscience, Maastricht University, Maastricht, The Netherlands. <sup>14</sup>New Mexico Veterans Affairs Healthcare System, Albuquerque, NM, USA. <sup>15</sup>O’Donnell Brain Institute, University of Texas Southwestern Medical Center, Dallas, TX, USA. <sup>16</sup>Steven and Alexandra Cohen Veterans Center for Post-traumatic Stress and Traumatic Brain Injury, New York University Langone School of Medicine, New York, NY, USA. <sup>17</sup>Center for Alcohol Use Disorder and PTSD, New York University Langone School of Medicine, New York, NY, USA. <sup>18</sup>Department of Psychiatry, New York University Langone School of Medicine, New York, NY, USA. <sup>19</sup>These authors contributed equally: Yu Zhang, Wei Wu.

the clinical utility of fMRI is limited due to substantial requirements in terms of expertise, specialized equipment and high cost, as well as persistent challenges harmonizing fMRI acquisition across scanners. By contrast, electroencephalography (EEG) is a less expensive neuroimaging technique, is easier to use in a variety of clinical environments and is thus a more practical tool for guiding clinical care. In this study, we therefore adopted EEG for subtyping analyses.

One challenge to analysis of functional connectivity using EEG, however, is the fact that nearby channel-space EEG signals, or their source estimates, typically share similar artefactual variance caused by electric field spread (that is, volume conduction), along with the limited spatial resolution of source localization methods<sup>20–22</sup>. This interferes with the extraction of neural patterns, such as functional connectivity, in an accurate manner using resting-state EEG (rsEEG) collected at the scalp<sup>23</sup>. To address this issue, a new method, power envelope connectivity (PEC), has been recently developed for estimating accurately the correlation structure of spontaneous oscillatory activity in magnetoencephalography (MEG)<sup>24,25</sup> and then validated for EEG<sup>26</sup>. PEC estimation mitigates spurious correlations resulting from volume conduction by removing signals with zero phase lag (that is, occurring non-physiologically simultaneously) through orthogonalization<sup>25–27</sup>. Of note, PEC was among the most reliable connectivity measures using MEG<sup>28</sup>. To this end, we sought biomarkers in PEC features extracted from source signals reconstructed from high-density rsEEG recordings.

As our primary goal was to delineate neurobiological heterogeneity in PTSD and MDD, rather than maximizing the differentiation of patients from healthy controls, we first defined EEG connectivity subtypes in patients. We then contrasted these connectivity patterns with healthy control connectivity, as well as assessed clinical significance with respect to prediction of clinical outcome with a variety of treatments. We used an unsupervised sparse-clustering approach<sup>29</sup> as a data-driven subtyping strategy that accomplished simultaneous feature selection and sample clustering on the high-dimensional PEC features (Supplementary Fig. 1). We implemented the same subtyping analysis on four independent datasets, including two different psychiatric disorders, PTSD and MDD. Discovery of these clinically relevant subtypes was first carried out on a PTSD discovery dataset involving 201 participants (106 with PTSD and 95 healthy controls), wherein a minority of patients were on concurrent psychiatric medications. This sample was chosen for discovery as it had the largest number of healthy controls, and it was the only dataset without clinical outcome data (which we used for determination of subtyping clinical significance). We then performed several replication analyses of the discovered subtypes: first, using two independent PTSD datasets with 72 and 63 patients each (many with concurrent medication use); and second, using two MDD datasets (with 228 patients that were medication free and 179 patients, many with concurrent medication use, respectively) to determine the transdiagnostic potential of our subtyping results. We also examined fMRI connectivity correlates of our subtypes across datasets to assess for convergent validation using a distinct neuroimaging modality. Finally, we tested for the clinical significance of our subtyping findings using a diverse range of clinical interventions, including patients with PTSD undergoing psychotherapy with either prolonged exposure (PE) or cognitive processing therapy (CPT), patients with MDD who were randomized to receive the selective serotonin reuptake inhibitor sertraline or placebo, and patients with MDD who received one of two repetitive transcranial magnetic stimulation (rTMS) treatment protocols as part of their clinical care along with psychotherapy.

## Results

**Resting-state EEG functional connectivity defines two clinically relevant subtypes.** To achieve data-driven subtyping on the discovery PTSD dataset (dataset 1), we combined PEC features from

all eight EEG conditions (four frequency bands across eyes-open/eyes-closed conditions) and submitted these to a sparse-clustering algorithm. Overwhelmingly, the selected features were from the beta frequency band and eyes-open condition (Fig. 1a). The two subtypes were characterized by strong connectivity differences in the frontal and posterior regions (Fig. 1b). The interhemispheric connectivity between homologous regions was also notable.

The most frequently occurring PEC differences involved regions located in the frontoparietal control network (FPCN) and the default mode network (DMN). Specifically, subtype 1 had stronger PEC between the frontal cortex and other regions but weaker PEC between the parietal cortex and other regions, compared with subtype 2 (Fig. 2a,b). A similar PEC feature pattern was observed for the subtypes when compared with those from other datasets (Supplementary Fig. 2). Importantly, no significant differences were observed in clinical severity between the two subtypes (Supplementary Fig. 3a). The only demographic difference was a higher percentage of males in subtype 1 (Supplementary Table 1).

On the entire patient population level, the mean connectivity matrix was highly correlated with that of the healthy controls (correlation coefficient  $r=0.96$ ,  $P < 10^{-5}$ ). However, when each subtype was inspected separately, while the mean connectivity matrices were highly similar between healthy controls and subtype 1 ( $r=0.94$ ,  $P < 10^{-5}$ ), the similarity was considerably lower between healthy controls and subtype 2 ( $r=0.44$ ,  $P < 10^{-5}$ ) (Fig. 1c).

**Replication in an independent PTSD dataset.** To test whether our subtype findings could be replicated, we implemented the same analysis on an independent rsEEG dataset consisting of 135 patients with PTSD who underwent rsEEG before receiving psychotherapy treatment (dataset 2). Dataset 2 contained two cohorts: 72 participants used for the initial submission of this paper and 63 participants who completed the study after our initial submission. The latter group thus allowed a further independent replication of clinical prediction effects tested for in the first cohort.

We first conducted a replication analysis for the identified subtype PEC pattern with each of the two cohorts, separately. Our subtyping method, using the same feature selection process as above, was again able to yield two clusters with differential functional connectivity in the beta band and eyes-open condition, consistent with results from the discovery PTSD dataset (Fig. 3a–d). Also, a similar PEC feature pattern was observed for the subtypes when compared with those from other datasets (Supplementary Fig. 2). In line with the discovery dataset, no significant difference in clinical severity was observed between the two subtypes (Supplementary Fig. 3b), and no differences in the proportion of males (Supplementary Table 1). Furthermore, in neither dataset 1 nor dataset 2 did concurrent use of psychiatric medications impact the subtyping result (Supplementary Fig. 4).

**Replication in two independent depression datasets.** We next investigated whether the discovered subtypes could serve as a potential transdiagnostic biomarker by applying the subtyping approach to two independent MDD datasets, involving either unmedicated patients with MDD ( $N=228$ ; dataset 3) or clinic-recruited patients with MDD, some of whom were on psychiatric medications ( $N=179$ ; dataset 4). Once again, two subtypes were observed with distinct functional connectivity patterns (Fig. 4a–d) that were consistent with those discovered in the two PTSD datasets. Consistent with the findings in the two PTSD datasets, a similar PEC feature pattern was observed for the subtypes when compared with those from other datasets (Supplementary Fig. 2). Likewise, no significant differences were observed in clinical severity between the two subtypes in either dataset (Supplementary Fig. 3c,d). Only in dataset 4 were males more common for subtype 2 (Supplementary Table 1). The transdiagnostic relevance of our subtyping findings were also

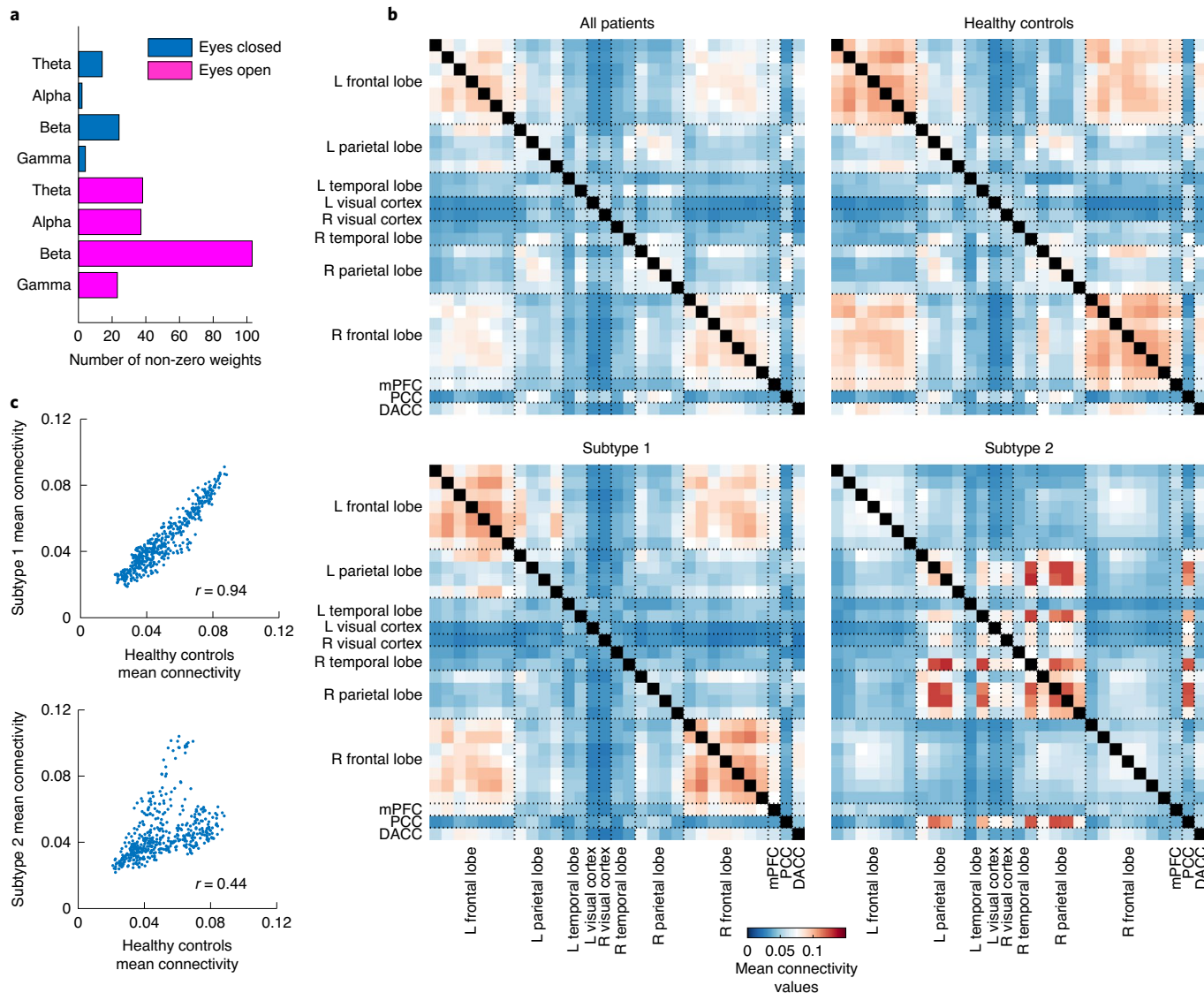


**Fig. 1 | Resting-state EEG PEC biomarkers define two subtypes in the discovery PTSD dataset.** PEC was calculated across pairs of 31 ROIs, separately for four frequency bands (theta, alpha, beta and gamma), as well as two resting conditions (eyes open and eyes closed). **a**, Number of non-zero feature weights for different conditions as a result of sparse clustering. Each feature weight corresponds to a PEC feature. Selected features are primarily from the beta frequency band and eyes-open condition. **b**, Mean connectivity matrices of all patients, healthy controls and two subtypes for the beta band and eyes-open condition. The colour bar indicates mean connectivity values. The black squares indicate that the diagonal elements in the connectivity matrices are non-meaningful for our analysis. L, left; R, right; DACC, dorsal anterior cingulate cortex. **c**, Correlation of mean connectivity between healthy controls and subtype 1, and between healthy controls and subtype 2, respectively. Each dot corresponds to the PEC between two ROIs. The scatterplots show that the mean connectivity patterns are highly similar between healthy controls and subtype 1, but less so between healthy controls and subtype 2.

seen when conducting clustering across all patients by pooling all four datasets (Supplementary Fig. 5).

**Validation of subtype transferability across datasets.** To assess the transferability of the discovered neurophysiological subtypes, we applied a cluster-centroid-based pattern classifier derived from the subtypes of one dataset to PEC features of another and compared the predicted subtype labels from the classifier with those obtained from clustering analysis of the second dataset. The classification accuracies averaged 90.6% and in all cases were greater than 86% (Fig. 5a). Furthermore, we iteratively trained the classifier on three of the datasets and tested on the fourth, which yielded an average of 89.9% accuracy, with all datasets greater than 88% (Fig. 5b). These results demonstrate that the discovered subtypes were transferable across independent datasets acquired using different

EEG equipment, using differing clinical diagnoses and patient identification methods, and recorded for different amounts of time. This conclusion was further supported by a permutation test of each dataset, which failed to reveal the observed subtypes in the original data (Supplementary Fig. 6). In addition, use of both the gap statistic criterion and Calinski–Harabasz criterion confirmed that two clusters are the optimal solution across datasets (Supplementary Fig. 7a,b). We also implemented a complementary analysis with the 26 channels that were comparable across all datasets (to match dataset 4). For each of datasets 1–3, we downsampled the channels to a subset (Supplementary Fig. 8a) and used the 26 channels that were most close to those of dataset 4 to rerun the source localization and PEC calculation. Then, we compared the consistency with which the subtype PEC pattern was observed in comparing between using all channels and the selected 26 channels. The results indicated

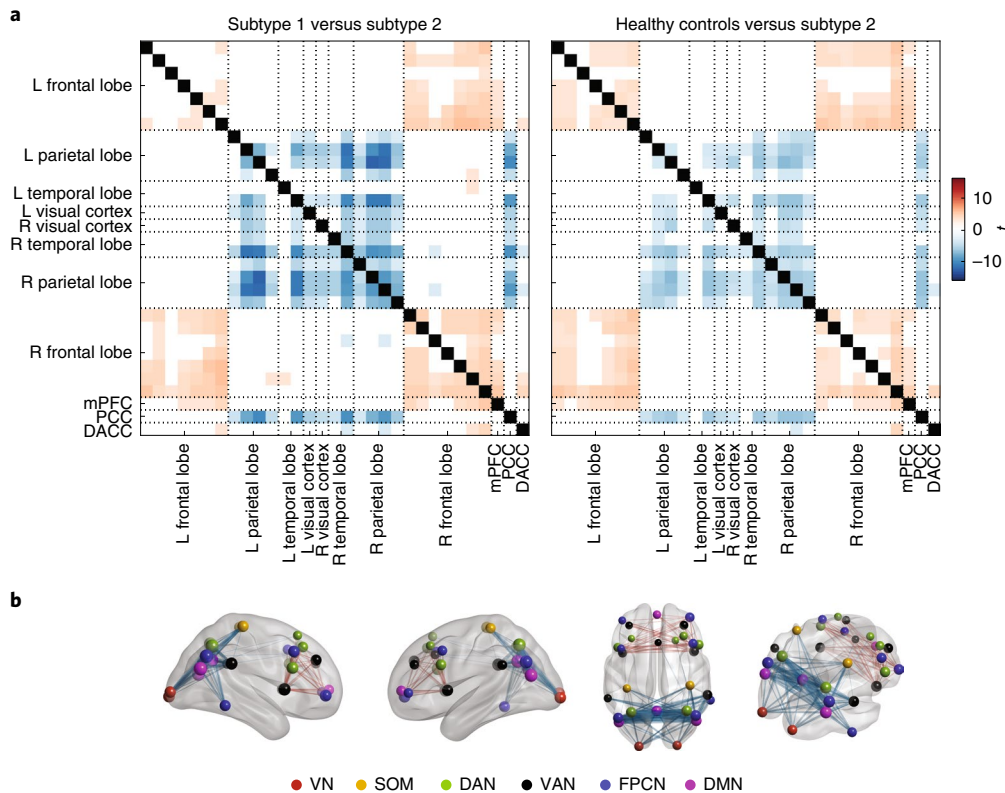


**Fig. 2 | PEC difference between the two subtypes.** **a**, Connectivity difference matrices for the beta band and eyes-open condition between the two subtypes and between healthy controls and subtype 2, assessed in a two-sample  $t$ -test (showing  $t$ -values with false discovery rate (FDR)-corrected  $P < 0.05$ ). **b**, Visualization of connectivity difference (subtype 1 versus subtype 2) patterns on the brain. The size of the sphere at each ROI represents the average  $t$ -value across all PEC features from that ROI to all others. Each edge represents the connectivity difference strength between two ROIs. VN, visual network; SOM, sensorimotor network; DAN, dorsal attention network.

that the subtype PEC pattern derived by the downsampled 26 channels was similar to that obtained using all channels for each of datasets 1–3 (Supplementary Fig. 8b). However, we still used all available channels for the experimental analysis since penalizing the three high-density datasets by the number of channels in the lowest-density dataset may discard potentially useful information.

**Clustering on healthy controls.** In addition to the patient subtyping analysis, we also implemented clustering on PEC features extracted from healthy controls of dataset 1. Similar subtype PEC patterns were observed in the healthy controls group to those found in the patient group (Supplementary Fig. 9a,b). However, subtype identity was less stable and more variable among healthy control compared with patient data (Supplementary Fig. 9c). In addition, it should be noted that the purpose of this study was to understand heterogeneity in patients, where it would have clinical significance. At present, the significance of these subtypes in healthy controls is unknown but may represent an underlying trait-like neurobiological feature.

**Subtype-based diagnostics.** To investigate how the discovered subtypes could mitigate heterogeneity and improve the diagnosis-based comparisons for a certain subtype, we applied the classifier derived from the sparse-clustering solution (Supplementary Methods) on datasets 2, 3 and 4 to PEC features of healthy controls from dataset 1, the only dataset where enough healthy controls are available, and investigated the misidentification rate of healthy controls for each subtype. The rate of healthy controls misidentified as subtype 2 was 21.0%, which was much lower than being misidentified as subtype 1 (79.0%). When both healthy controls and patients were considered, the overall rate of a participant misidentified as subtype

2 was 15.2%, achieving an identification rate of subtype 2 with a sensitivity of 89.2% (Fig. 5b). These results suggest that identifying heterogeneous EEG-based subtypes in psychiatric patients might enhance differentiation from healthy controls, though this was not the primary goal of this study.

**Further validation based on fMRI connectivity.** To further validate that our identified subtypes indeed represent internally valid and neurobiologically meaningful phenotype related to brain connectivity, we carried out a classification analysis to distinguish the two EEG-connectivity-defined subtypes using resting-state fMRI (rsfMRI) connectivity features, pooling across fMRI data in datasets 1–3. Our classifier with rsfMRI was able to distinguish the two EEG-connectivity-driven subtypes with an accuracy of 83.9% (permutation test,  $P < 0.0001$ ), a sensitivity of 85.7% in detecting subtype 1 and 81.2% in detecting subtype 2 (Supplementary Fig. 10a). The most discriminative features involved regions of the FPCN, ventral attention network (VAN) and visual network (Supplementary Fig. 10b). By comparing the PEC difference and fMRI connectivity classifier profiles, we observed a consistent pattern between PEC and fMRI connectivity in distinguishing the two EEG subtypes (Supplementary Fig. 10c). Here, 90 out of 465 connections are overlapping and a consistent pattern is observed between EEG and fMRI, mainly involving the FPCN, DMN and VAN regions. These results further provide strong evidence to support the convergent validation of our PEC-defined subtype findings.

**Responsiveness of subtypes to treatment.** Finally, and especially considering the lack of clinical severity differences between the subtypes before treatment, we sought to determine whether the two

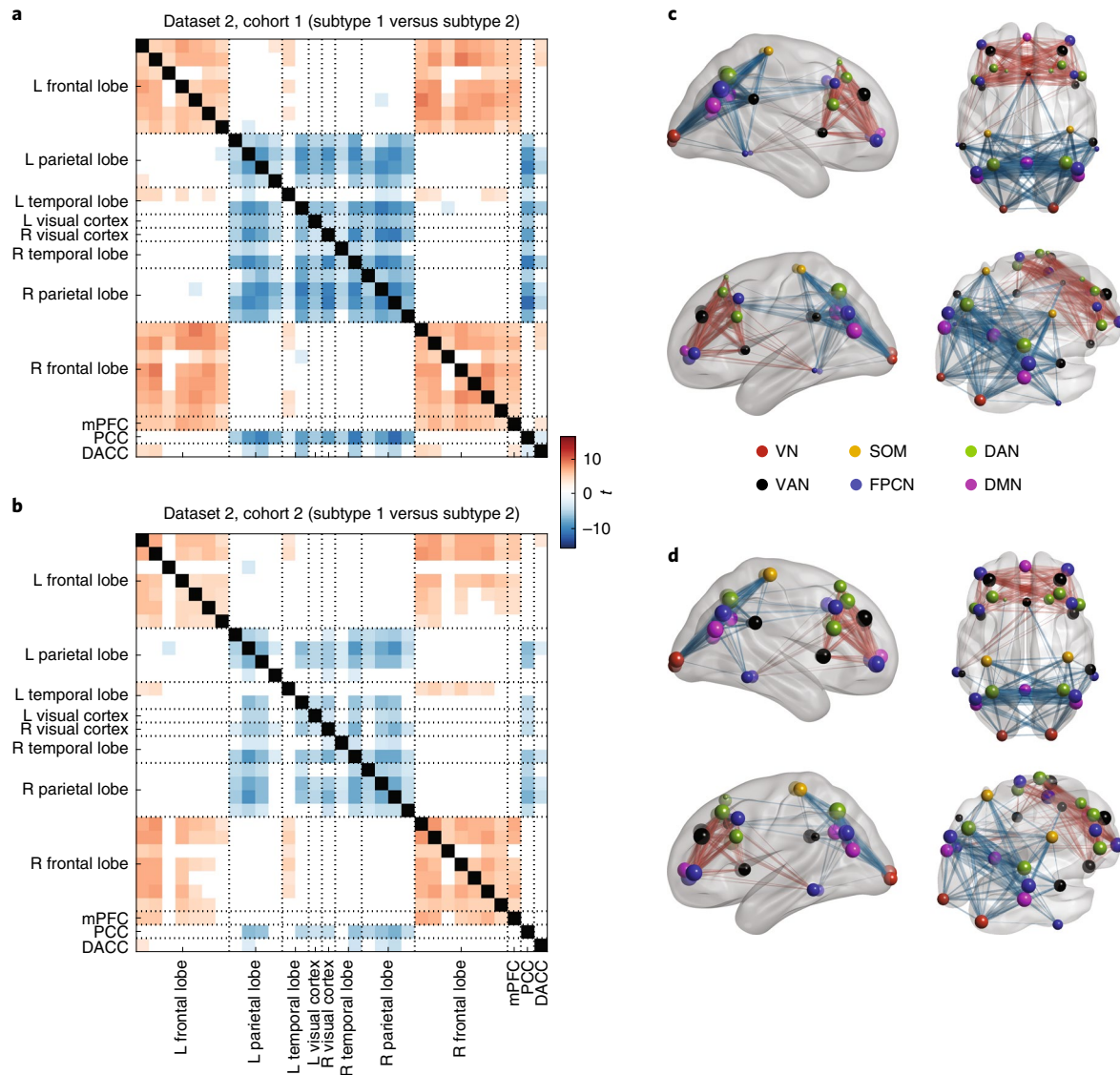


**Fig. 3 | Replication of the identified PEC subtypes in the two cohorts within dataset 2 (PTSD replication).** For each cohort, connectivity difference was assessed in a two-sample t-test with subtype 1 versus subtype 2 (showing  $t$ -values with FDR-corrected  $P < 0.05$ ). **a,b,** Connectivity difference matrix obtained from the first (**a**) and the second (**b**) cohorts. **c,d,** Visualization of connectivity difference patterns on the brain for the first (**c**) and the second (**d**) cohorts. For both cohorts in dataset 2, two subtypes were found with highly similar patterns of functional connectivity differences to those in the discovery dataset.

subtypes held clinical significance by examining treatment outcome data, which were available in the three replication datasets.

Patients in the PTSD replication cohort (dataset 2) received either PE or CPT, which are at present the most evidence-based treatments for PTSD. We divided the dataset into two cohorts: 72 participants used for the initial submission of this paper and 63 participants who completed the study after the initial submission (and thus information on which was not available with our first submission). Using linear mixed models in an intent-to-treat analysis on clinician-rated PTSD severity (Clinician-Administered PTSD Scale (CAPS)) that incorporated both completers and dropouts, we found that subtype 1 had a better treatment outcome compared with subtype 2 (Group  $\times$  Time interaction:  $F(1,123)=9.04$ ,  $P=0.0032$ , Cohen's  $d=0.80$  for CAPS-IV and  $F(1,123)=4.38$ ,  $P=0.039$ , Cohen's  $d=0.59$  for CAPS-5; Fig. 6a). If further dividing by psychotherapy type, subtype 1 had a significantly better outcome across both treatments, as well as separately for PE ( $F(1,38)=7.23$ ,  $P=0.011$  for CAPS-IV and  $F(1,38)=2.90$ ,  $P=0.097$  for CAPS-5) and for CPT

( $F(1,81)=4.75$ ,  $P=0.032$  for CAPS-IV and  $F(1,81)=2.41$ ,  $P=0.12$  for CAPS-5). To further replicate the response of the subtypes to psychotherapy treatment, we applied the subtyping analysis to the second cohort followed by linear mixed model effect analyses. Consistent with those observed on the first cohort, subtypes status in the second cohort similarly predicted responsiveness to the psychotherapy treatment, with subtype 1 responding significantly better than subtype 2 (Group  $\times$  Time interaction:  $F(1,109)=4.76$ ,  $P=0.031$ , Cohen's  $d=0.56$  for CAPS-IV and  $F(1,109)=4.46$ ,  $P=0.037$ , Cohen's  $d=0.55$  for CAPS-5; Fig. 6b). When separating patients by treatment arms, we observed a significant response difference between the subtypes for PE ( $F(1,34)=3.09$ ,  $P=0.088$  for CAPS-IV and  $F(1,34)=9.31$ ,  $P=0.0044$  for CAPS-5) and a marginally significant difference in the expected direction for CPT ( $F(1,71)=2.13$ ,  $P=0.15$  for CAPS-IV and  $F(1,71)=0.74$ ,  $P=0.39$  for CAPS-5). To assess the strength of our subtype findings on predicting treatment response, we compared the percentage of responders between the two subtypes. Subtype 1 included significantly more

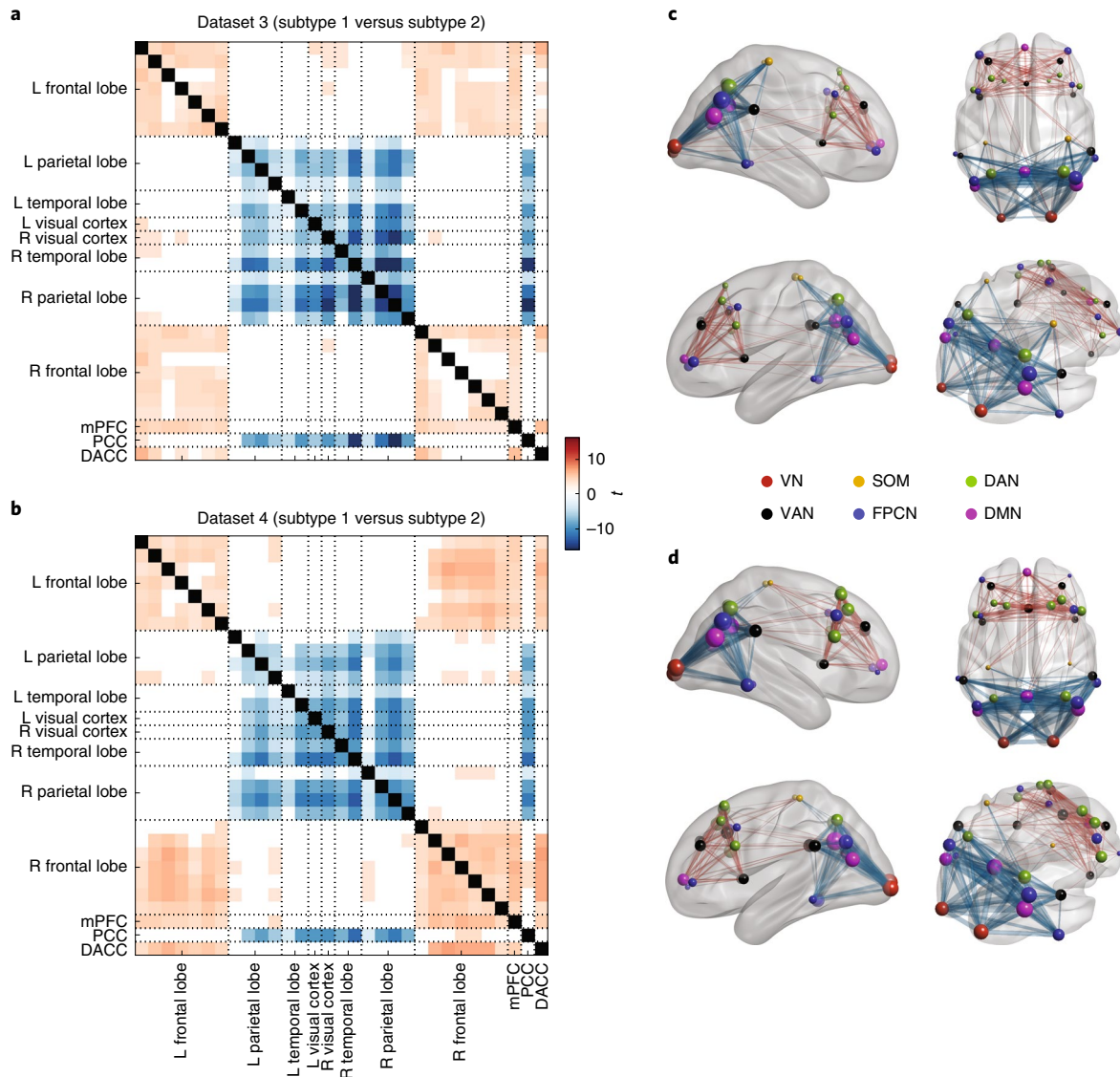


**Fig. 4 | Replication of the identified PEC subtypes in the two MDD datasets.** For each dataset, connectivity difference was assessed in a two-sample *t*-test with subtype 1 versus subtype 2 (showing *t*-values with FDR-corrected  $P < 0.05$ ). **a,b**, Connectivity difference matrix obtained from dataset 3 (**a**) and dataset 4 (**b**). **c,d**, Visualization of connectivity difference patterns on the brain for dataset 3 (**c**) and dataset 4 (**d**). Two subtypes were discovered with distinct functional connectivity patterns that were consistent with those found in the two PTSD datasets.

responders with PTSD than those in subtype 2 for psychotherapy treatment ( $X^2 = 4.07$ ,  $P = 0.044$ , with a number needed to treat of 5.1 for CAPS-IV; Supplementary Fig. 11a).

One of the MDD replication cohorts (dataset 3) was randomized post-EEG to receive either the antidepressant sertraline or placebo. Linear mixed models on clinician-rated depression severity (Hamilton Depression Rating Scale (HAMD<sub>17</sub>)) in an intent-to-treat analysis revealed that the two subtypes differed in their response to sertraline versus placebo (Fig. 6c). Specifically, while sertraline was significantly better than placebo for patients in subtype 1 (Group  $\times$  Time interaction:  $F(1,851) = 6.38$ ,  $P = 0.012$ ), the two arms failed to separate for patients in subtype 2 ( $F(1,517) = 0.093$ ,  $P = 0.76$ ). The treatment response analysis revealed that for sertraline, subtype 1 included significantly more responders with MDD than those in subtype 2 for antidepressant medication ( $X^2 = 4.49$ ,  $P = 0.034$ , and the number needed to treat is 4.2). However, for placebo, there was no significant difference ( $X^2 = 0.041$ ,  $P = 0.84$ ) in the number of responders between the two subtypes (Supplementary Fig. 11b).

We further tested for subtype-related differences in treatment outcome to rTMS concurrent with psychotherapy, which was given using one of two protocols to the patients in the second MDD replication cohort (dataset 4; 10 Hz to the left dorsolateral prefrontal cortex (DLPFC) or 1 Hz to the right DLPFC). Linear mixed models on self-reported depression severity (Beck Depression Inventory (BDI)) in an intent-to-treat analysis showed an effect of time for either rTMS protocol ( $F(1,142) > 27$ ,  $P < 0.00001$  for 10 Hz and  $F(1,207) > 22$ ,  $P < 0.00001$  for 1 Hz), but no difference between subtypes in either protocol ( $F(1,142) = 1.5$ ,  $P = 0.22$  for 10 Hz and  $F(1,207) = 0.01$ ,  $P = 0.92$  for 1 Hz, Fig. 6d). A Bayes factor analysis<sup>30</sup> was also used to quantify support for the null hypothesis of no differential treatment outcomes with rTMS between subtypes. We obtained Bayes factor  $BF_{10} = 0.23$  for alternative hypothesis ( $H_1$ ) versus null hypothesis ( $H_0$ ). A  $BF_{10}$  value above 1 indicates evidence for alternative hypothesis over null hypothesis, whereas a value below 1 indicates the opposite. Conventionally, the strength of evidence is at least moderate for null hypothesis over alternative hypothesis when  $BF_{10}$  is in the range 0.1–0.33. Thus, the Bayes factor result

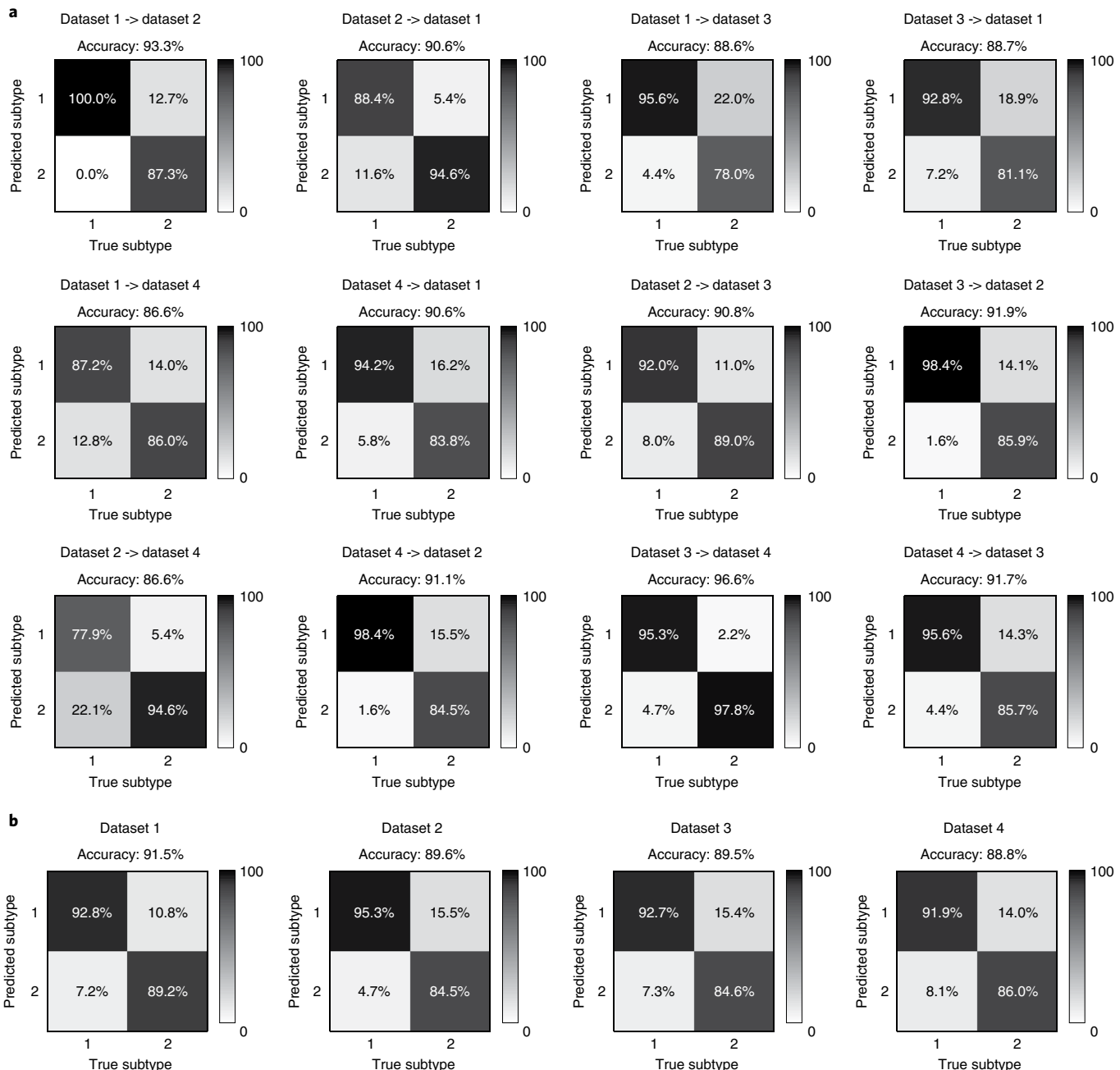


**Fig. 5 | Validation of subtype transferability across independent datasets.** A cluster-centroid-based classifier was derived from the sparse-clustering analysis from one dataset (using PEC features from beta band and eyes-open condition) and then applied to data from another independent dataset, resulting in predicted class labels. Classification accuracy was then calculated by comparing the predicted class labels with those obtained from the sparse-clustering analysis on the second dataset. **a**, Training on one dataset and tested on one other. **b**, Training on three datasets and tested on the fourth (test set noted in the title of each set of results).

provided further support for the lack of treatment outcome difference between subtypes.

In summary, by contrast to baseline clinical measures, on which the subtypes did not differ, their response to treatment on the same measures differed strikingly across a variety of treatments. Moreover, whereas the subtypes differed in their response to psychotherapy and antidepressant medication, the two subtypes responded similarly to each of two different protocols in the concurrent rTMS with psychotherapy treatment study. We also report the results of these treatment prediction analyses on item-level clinical scores in Supplementary Tables 2–4.

**Clustering on clinical scores.** To confirm that our subtype findings were specific to EEG, we also clustered the clinical scores and demographic information alone. For each dataset, the baseline item-level clinical scores and demographic variables (that is, age, gender and years of education) were used as the features for clustering to generate clinical subtypes. The number of clusters was assessed using gap statistic criterion<sup>31</sup> (Supplementary Fig. 12a). By contrast with the replicable subtypes derived from PEC features, the clinical/demographic features identified three subtypes in discovery PTSD dataset 1, but no subtypes in replication PTSD dataset 2. Likewise, no clinical subtypes were found on MDD dataset 3, while two

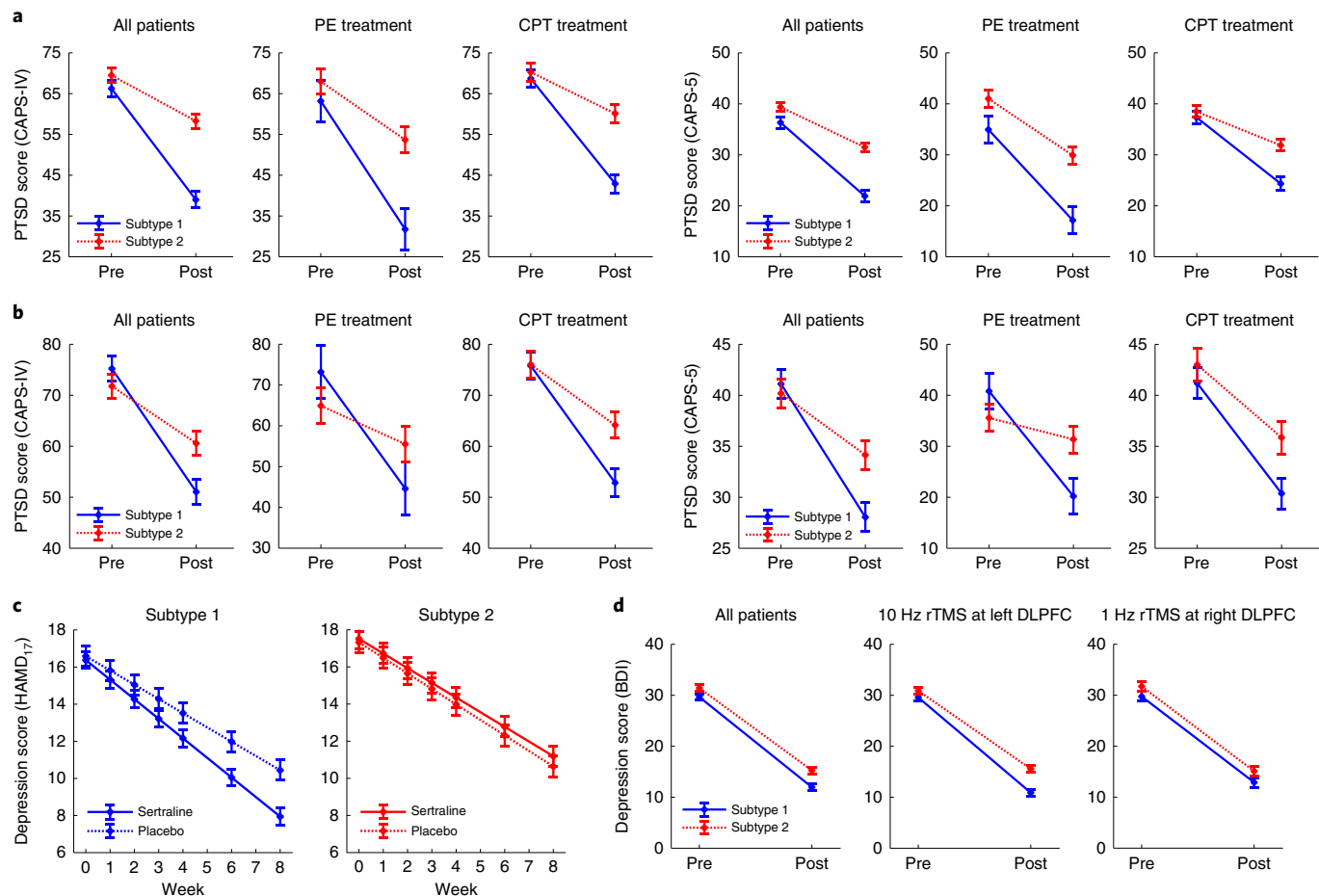


**Fig. 6 | Responsiveness of subtypes to treatment across diagnoses and treatment modalities.** **a**, Patients in subtype 2 had worse outcomes to psychotherapy treatment in PTSD for the first cohort of dataset 2. **b**, Similarly, patients in subtype 2 responded significantly worse than patients in subtype 1 to psychotherapy treatment in PTSD in the second cohort of dataset 2. **c**, Patients in subtype 2 failed to respond differentially to an antidepressant versus placebo in MDD (dataset 3), whereas for patients in subtype 1 the antidepressant was superior to placebo. **d**, Patients in both subtypes responded equally well to one of the two different rTMS treatment protocols in MDD (dataset 4). All error bars indicate the standard error of the mean.

subtypes were identified using clinical features in MDD dataset 4 (Supplementary Fig. 12b). That is, clustering on clinical and demographic variables demonstrated that our replicable disease subtypes using PEC features could not be discovered using clinical measures alone. The results confirmed that the EEG connectivity subtyping capitalized on neural information that was not available in the standard clinical and demographic variables.

## Discussion

A central limitation of much neuroscience research in psychiatry has been that patients have been considered as a unitary group for which a maximally sensitive way to differentiate them from controls is needed. Evidence suggests that studying case-control group differences may impede psychiatric biomarker discovery and an understanding of psychiatric pathophysiology, due to the intrinsic heterogeneity in neurobiological abnormalities within current clinical definitions for diagnoses<sup>3,4,32</sup>. Moreover, how biomarkers that can elucidate this heterogeneity are to be identified, and replicated, has remained a long-standing challenge<sup>33</sup>. In this study, we have taken the perspective that finding the best way to describe biological heterogeneity in patients through data-driven approaches will help inform the best questions to ask with respect to clinical outcomes and relationship to healthy controls<sup>4</sup>. Here we implemented a data-driven neurobiological analysis by examining PEC-based signals from rsEEG, which led to discovery of two replicable

disease subtypes, based on primarily eyes-open beta-band connectivity differences, and evident across two major psychiatric populations (that is, PTSD and MDD). While these two subtypes did not differ in terms of baseline clinical severity in any of the four datasets studied, they did differ in terms of clinical outcome with respect to either psychotherapy (for PTSD, which we furthermore replicated) or treatment with an antidepressant versus placebo (for MDD). In particular, subtype 2, whose PEC patterns were more distinct from those of healthy controls, responded less well to both treatments. By contrast, treatment with rTMS concurrent with psychotherapy was equally effective in both subtypes (for MDD). Moreover, the finding of different predictors of response to medication versus rTMS draws further support from our previous work, as well as that of others. Most notably, more intact DMN connectivity in the iSPOT-D study predicted better treatment outcome with antidepressant treatment<sup>34</sup>, while more perturbed DMN connectivity predicted better outcome with rTMS<sup>35</sup>. Unlike previous work, however, here we included a placebo medication arm, demonstrating that the subtypes differ in medication response relative to placebo as well. Thus, our findings are relevant for the identification and potential clinical translatability of psychiatric disease subtypes.

Subtype 1 was also found to have a PEC pattern more similar to that of healthy controls. Our interpretation of subtype 1, consistent with a long history of findings in psychiatric neuroimaging, is that on any given measure there are many patients who are equally

symptomatic but do not demonstrate a biological abnormality relative to healthy controls. Not doing so on one measure (EEG connectivity in our case) does not, however, mean that they do not differentiate from healthy controls on other measures. Importantly, though, the fact that we could differentiate the two subtypes in a purely data-driven manner that made no reference to healthy control EEG connectivity, and that one subtype overlapped highly with controls while the other did not, makes a strong statement in particular about the relevance of identifying the subtype that ended up differing from controls and responding poorly to psychotherapy and antidepressants.

A fundamental challenge in discovering biomarkers for psychiatric conditions is the accurate identification of those features most relevant to understanding a particular clinical population. We extracted PEC from source-localized rsEEG as the features for biomarker discovery. PEC computation has proven to be effective for mitigating the effects of volume conduction, a major shortcoming of EEG data, thereby accurately capturing neurobiologically meaningful connectomic information within different frequency bands of spontaneous oscillatory activity<sup>36</sup>. Using this method, a previous study from our group used PEC to investigate connectivity abnormalities in PTSD patients versus healthy controls as a group-wise comparison<sup>27</sup>. Doing so revealed a PTSD-related connectomic difference almost exclusively in eyes-open theta-band PEC. Those results differ from the present work on two critical fronts—that the present analysis focuses on a data-driven dissection of heterogeneity rather than identifying group-level differences based on clinical categories, and as a consequence that the resulting PEC features have no overlap.

Since different frequency bands and EEG resting-state paradigms (for example, eyes open and eyes closed) may carry different neurobiological information, which condition possesses the most informative features for subtype identification is unknown *a priori*. Instead of analysing each condition separately, we employed a sparse-clustering<sup>29</sup> approach to implement simultaneous feature selection and clustering by maximizing the between-cluster dissimilarity with a sparsity constraint on the PEC features. This data-driven approach identified that PEC features from the beta-band eyes-open condition were the most informative biomarkers for delineating the two discovered subtypes. Beta-band PEC in previous MEG and simultaneous EEG-fMRI work is best able to yield large-scale functional networks with spatial features qualitatively and quantitatively similar to rsfMRI networks<sup>37,38</sup>. In our data, the beta-band eyes-open condition yielded two subtypes characterized by strongly divergent PEC patterns in the frontal and posterior regions, respectively. Interestingly, the mean PEC patterns across either all patients or healthy controls resembled previously reported group-level healthy control beta-band PEC patterns in MEG studies<sup>28,39</sup>. Although the mechanism mediating the two divergent connectivity patterns we discovered remains unclear, computational models may be employed to shed light on the possible scenarios that may account for PEC patterns similar to those we observed<sup>39,40</sup>. For instance, a model of coupled oscillators was used to study the source of the amplitude fluctuations observed in resting MEG signals of healthy participants, where good agreement between the simulated and actual amplitude envelope connectivity patterns was achieved with proper coupling strengths and temporal delays between regions<sup>39</sup>. This model may help us understand factors that give rise to the distinct PEC patterns of the two subtypes.

Of note, unlike other previous studies, which focused only on *a priori* regions of interest or which selected features based on their correlation with clinical symptoms<sup>41</sup>, our connectivity biomarker discovery was based purely on EEG data without assuming any prior knowledge about individual brain regions, frequency bands or resting-state paradigms. Consequently, this feature selection eschewed the potential bias due to a selective focus on brain regions

that were thought to contribute to the pathophysiology of psychiatric disorders, which, however, might not be optimal for subtype identification. Moreover, our finding generalized across distinct datasets, which used different clinical criteria (and for different diagnoses), had variable rates of concurrent medication use, as well as used different EEG equipment (including amplifiers, channel count and montages).

Using the sparse-clustering-based data-driven approach, we found that the most informative PEC features were located in regions that contribute to the FPCN and the DMN. Specifically, subtype 1, which had stronger beta-band PEC in frontal regions but weaker beta-band PEC in parietal regions relative to subtype 2, gained significantly greater clinical benefit from either psychotherapy or antidepressant medication (versus placebo). In accordance with our findings, previous fMRI studies<sup>42–47</sup> have reported that functional connectivity abnormalities in the FPCN and the DMN were associated with the treatment outcome of psychotherapy in various psychiatric disorders. Specifically, lower pre-treatment functional connectivity in the cognitive control network including the DLPFC and the anterior cingulate cortex (ACC) was found to predict poorer antidepressant outcome<sup>42</sup>. A whole-brain voxel-wise analysis on rsfMRI revealed that treatment response to cognitive behavioural therapy in generalized social anxiety disorder was predicted by amygdala–prefrontal connectivity<sup>43</sup>. Stronger DLPFC activity and DLPFC–cerebellum connectivity during a working memory task at baseline was found to be strongly associated with a favourable response to cognitive behavioural therapy in schizophrenia<sup>44</sup>. Pre-treatment within-DMN connectivity was observed to predict post-treatment symptom severity of obsessive-compulsive disorder after cognitive behavioural therapy<sup>45</sup>. Pre-treatment DMN connectivity was also observed to contribute significantly to the multivariate pattern analysis for predicting clinical responses to antidepressant medication<sup>46</sup>. A randomized controlled trial also revealed that pre-treatment connectivity between the posterior cingulate cortex (PCC) and the ACC/medial prefrontal cortex (mPFC) predicted remission on antidepressant<sup>47</sup>. In addition, deactivation of the precuneus and PCC in DMN during an emotion discrimination task was observed to predict treatment outcome of antidepressant medication<sup>48</sup>. Furthermore, greater MEG connectivity between the DLPFC and the ACC in the alpha band at baseline was found to predict better antidepressant treatment<sup>49</sup>. Pre-treatment EEG beta connectivity in frontal regions was reported to be positively correlated with clinical score change in MDD<sup>50</sup>. The similarities in the key regions identified in our EEG subtyping analysis and those previously reported in treatment prediction studies by fMRI are further echoed by regions with fMRI connectivity differences we observed in our data when dividing patients by their EEG-determined subtypes.

Our findings also suggest that rTMS-based neurostimulation treatment may provide a promising approach for treating patients who are otherwise less responsive to treatment<sup>51</sup>. Although subtype 2 was shown to be less responsive to psychotherapy and antidepressant medication, our rTMS findings demonstrated that both subtype 1 and subtype 2 responded similarly to two different rTMS treatment protocols (left prefrontal 10 Hz and right prefrontal 1 Hz). This suggests that neurostimulation may be a good option relative to psychotherapy and antidepressant medication for subtype 2. In other words, our identified neural ‘medication/psychotherapy resistance’ phenotype may be separate from brain features that mediate responsiveness to rTMS with concurrent psychotherapy, and thus patients in subtype 2 may be better served clinically by advancing faster to rTMS. It is typical that patients receive multiple rounds of pharmacological treatment for years, resulting in substantial morbidity and economic cost, before resorting to a treatment modality such as rTMS<sup>52,53</sup>. Even then, only a small minority of patients with depression who are resistant to treatment receive rTMS. More

rapidly advancing patients with an antidepressant-non-responsive brain phenotype to rTMS, despite the cost of this procedure, may thus make both clinical and financial sense<sup>52–55</sup>, while medication trials may be preferred for patients with an antidepressant-responsive brain phenotype. In this vein, it is worth noting that the large-scale studies of rTMS treatment for depression have specifically enroled medication-resistant patients, and benefit has been shown for real over sham rTMS<sup>54,55</sup>. For this suggestion to be directly demonstrated, however, studies directly comparing rTMS to medication or psychotherapy based on patient subtype are needed. Likewise, it is important to note that patients receiving rTMS in dataset 4 also received psychotherapy, and thus it is not possible to know whether the similar outcome between subtypes was solely due to rTMS or its combination with psychotherapy.

Several limitations and potential extensions of the present study are important to note. First, our subtype findings on predicting responsiveness to psychotherapy and antidepressant medication remain to be replicated in additional independent PTSD and MDD samples with the same types of treatment. Second, here the fourth dataset used 26 EEG channels, which is generally considered low for source reconstruction and this may in turn affect subtyping performance<sup>56</sup> (though we observed similar classification rates as for the other datasets). Third, despite the fact that orthogonalization removes the zero-lag connectivity, PEC still suffers from ghost connectivity resulting from volume conduction in the vicinity of true connectivity<sup>57</sup>. Moreover, as a bivariate connectivity metric, PEC is inherently vulnerable to spurious links due to the common effects of a third neural source<sup>58</sup>. Subtype identification may be further refined (including with respect to the number of subtypes identified) using other EEG connectivity measures that may capture different aspects of brain connectivity (for example, imaginary coherence<sup>59</sup>, weighted phase lag index<sup>60</sup>, Granger causality<sup>61</sup>, directed transfer function<sup>62</sup> and partial directed coherence<sup>63</sup>). Likewise, the relevance of our findings for other types of psychiatric diagnoses, such as schizophrenia, autism or addiction is unknown. Finally, the present study assumes the connectivity patterns to be static over time, and hence is unable to disentangle their temporal dynamics, which however may be crucial for understanding of functional communication in mental disorders<sup>64</sup>.

In summary, we identified neurobiological biomarkers of clinically relevant subtypes from rsEEG PEC using a sparse-clustering-based data-driven approach to elucidate critical heterogeneity in psychiatric populations. Our extensive samples and analyses revealed that the discovered PEC biomarkers from the beta band and eyes-open condition delineated two stable and replicable clinically relevant subtypes that crossed traditional diagnostic boundaries. The two subtypes did not differ in terms of baseline clinical severity in any dataset but were associated with both critical differences and similarities in subsequent clinical outcome with a broad range of clinical interventions. Accordingly, our subtype findings provide a generalizable approach for defining treatment-relevant neurobiological heterogeneity in psychiatric populations.

## Methods

**PTSD study dataset 1. Participants.** Our discovery study involved 201 participants, including 106 individuals with PTSD and 95 healthy participants who had been exposed to trauma<sup>27</sup> (Supplementary Table 5). All participants were combat veterans serving during the Operation Iraqi Freedom (Iraq), Operation Enduring Freedom (Afghanistan) and Operation New Dawn periods. Participants were recruited and assessed at either Stanford University or New York University after signing an informed consent approved by the relevant university's institutional review board, in accordance with the ethical principles in the Declaration of Helsinki. Psychiatric diagnoses were based on the Diagnostic and Statistical Manual of Mental Disorders (DSM)-V criteria using CAPS<sup>5</sup>, and for other diagnoses using the Structured Clinical Interview for DSM-IV (SCID)<sup>66</sup>. All diagnoses were confirmed in consensus clinician meetings. A history of traumatic brain injury was determined based on whether loss of consciousness occurred after a combat-related head trauma. In addition to the CAPS and SCID, participants

completed the BDI to assess depressive symptoms, and the World Health Organization Quality of Life Scale (WHOQOL) to assess functioning. General exclusion criteria for both groups included the following: a history of psychotic, bipolar or active substance dependence (within three months for patients and lifetime for controls). Healthy controls who had been exposed to trauma were required to have experienced a criterion A trauma, but not meet lifetime criteria for any axis 1 psychiatric disorder, including PTSD.

**Resting-state EEG acquisition.** EEG data of the discovery PTSD dataset were collected using a BrainAmp d.c. amplifier (Brain Products) at a sampling rate of 5 kHz with the analogue bandpass filtering between 0 and 1 kHz. Following the standard 10–20 system, the Easy EEG cap with 64 Ag/AgCl electrodes were used for the data recordings. The reference electrode was attached to the tip of the nose. During the experiment, participants were seated on a comfortable chair and instructed to remain awake and complete two sessions (three-minute eyes-closed and three-minute eyes-open paradigms).

**Resting-state EEG pre-processing.** The recorded rsEEG data were cleaned offline with our in-house fully automated artefact rejection pipeline, thereby minimizing the biases in pre-processing possible with manual rejection of artefacts. The steps are briefly described as follows. (1) The EEG data were resampled to 250 Hz. (2) The 60 Hz a.c. line noise artefact was identified via the Thompson F-statistic and removed by a multi-taper regression technique<sup>67</sup>. (3) Non-physiological slow drifts in the EEG recordings were removed using a 0.01 Hz high-pass filter. (4) Bad epochs were rejected by thresholding the magnitude of each epoch. Bad channels were rejected based on thresholding the spatial correlations among channels. Subjects with more than 20% bad channels were discarded. The rejected bad channels were then interpolated from the EEG of adjacent channels via the spherical spline interpolation<sup>68</sup>. (5) Remaining artefacts were removed using independent component analysis<sup>69</sup>. Independent components related to the scalp muscle artefact, ocular artefact and ECG artefact were automatically rejected using a pattern classifier trained on expert-labelled independent components from another independent EEG dataset. (6) EEG data were re-referenced to the common average. The resulting EEG data were then filtered into four canonical frequency ranges: theta (4–7 Hz), alpha (8–12 Hz), beta (13–30 Hz) and low gamma (31–50 Hz).

**Resting-state fMRI acquisition.** Resting-state fMRI was collected from each participant for eight minutes. Participants were scanned using either a General Electrical 750 scanner at Stanford University or a Siemens 3T Skyra scanner at New York University. Both sites acquired 32 axial slices with 3.5 mm thickness using an echo-planar gradient-epoch T2-weighted pulse sequence (with 2,000 ms repetition time, 29 ms echo time, 90° flip angle, 0 slice spacing, 20 cm field of view, 64 × 64 matrix size). A high-resolution T1-weighted structural scan was acquired using three-dimensional MPGRAGE in the sagittal plane with parameters: inversion time 450 ms, repetition time 8.21 ms, echo time 3.22 ms, flip angle 15°, field of view 24 cm, 184 slices, matrix size 256 × 256, acquired resolution 0.9375 × 0.9375 × 1.0 mm<sup>3</sup>. The quality of fMRI scans was monitored by MRI centre staff weekly with scans of a Functional Biomedical Informatics Research Network (fBIRN) agar phantom, as described in previous literature<sup>70</sup>.

The following text is reproduced from our previous publications<sup>11,19</sup>. As this was a two-site study, before study initiation, we harmonized image acquisition sequences across the two scanners. This involved assessing both the image quality and the signal-to-noise ratio of images acquired using different parameters at each site, as well as acquisition of the same sequences on several travelling non-study control participants. Scanning of travelling non-study controls was repeated at roughly mid-study. Though the same acquisition sequences were used at both sites, differences between scanners are expected. For example, the echo-planar resting-state scans typically had more ventral prefrontal and temporal lobe susceptibility-artefact dropout at the Stanford University site than the New York University site. These differences in acquisition site were accounted for using a site variable in all statistical models. During the progress of the study, assessment of signal quality and stability was done as follows. For each scan, quality was assessed by quantitative and qualitative factors, with results regularly reported to MRI centre staff and principal investigators at weekly meetings. Quantitative factors include: scan parameters (check for correctness), slice-based signal-to-noise ratio and total root mean square head motion, as well as framewise displacement. We also monitored scanner performance by tracking reference voltage, imaging frequency and bias field correction over time. Reference voltage (also known as radio-frequency transmit reference voltage) determines the amplitude of the radio-frequency pulses. Imaging frequency variations can indicate scanner problems. The scanner's central frequency is typically set to the resonance frequency of water photons. Measurements of this are proportional to the field strength, and imaging frequency is a common calibration parameter and can be found in every image's DICOM header. Variations that exceed reference values can indicate magnet drift or radio-frequency instability. Qualitative factors were assessed visually by a trained image-quality assessor. These included field of view clipping, wrapping, dropout, ringing/stripping, blurring, ghosting, radio-frequency problems (noise, spikes, leakage) and inhomogeneity.

**Functional MRI pre-processing.** The fMRI pre-processing was performed using fMRIPrep<sup>71</sup>. The T1-weighted image was corrected for intensity non-uniformity and then skull-stripped. Brain tissue segmentation of cerebrospinal fluid, white matter and grey matter was performed on the brain-extracted T1-weighted image using FSL<sup>72</sup>. Volume-based spatial normalization was performed through nonlinear registration using brain-extracted versions of both the T1-weighted image and template. For each fMRI scan, the following pre-processing was performed. First, a reference volume and its skull-stripped version were generated using a custom methodology of fMRIPrep. A deformation field to correct for susceptibility distortions was estimated based on fMRIPrep's fieldmap-less approach. Registration is performed with antsRegistration, and the process regularized by constraining deformation to be non-zero only along the phase-encoding direction, and modulated with an average fieldmap template. Based on the estimated susceptibility distortion, a corrected echo-planar imaging reference was calculated for a more accurate co-registration with the anatomical reference. The blood-oxygenation-level-dependent (BOLD) reference was then co-registered to the T1-weighted image. Co-registration was configured with 12 degrees of freedom to account for distortions remaining in the BOLD reference. Head-motion parameters with respect to the BOLD reference are estimated before any spatiotemporal filtering. BOLD signals were slice-time corrected and resampled onto their original space by applying a single, composite transform to correct for head-motion and susceptibility distortions. The BOLD signals were then spatially normalized into the standard space. Automatic removal of motion artefacts using independent component analysis was performed on the pre-processed BOLD on the Montreal Neurological Institute space time series after removal of non-steady state volumes and spatial smoothing with an isotropic, Gaussian kernel of 6 mm full-width half-maximum.

**PTSD study dataset 2. Participants and treatment.** The replication PTSD dataset includes 135 participants (Supplementary Table 6) recruited based on meeting clinical criteria for PTSD in the context of evaluation for psychotherapy treatment in a Veterans Affairs clinic located in either Northern California or New Mexico. This dataset contains two cohorts: 72 participants used for our initial submission and 63 participants who completed the study after our initial submission (and thus can serve as an additional opportunity for replication analyses). Written informed consent was obtained from each participant under institutional-review-board-approved protocol at Stanford University. All assessments occurred at Stanford, with participants recruited in New Mexico being flown, after signing a local written informed consent, to Stanford. Exclusion criteria followed those in dataset 1. Clinical severity was assessed using the CAPS interview for both DSM-IV and DSM-5, using self-reported BDI and WHOQOL.

After baseline assessment, participants were enrolled to one of two evidence-based manualized protocols for the treatment of PTSD: (1) PE<sup>73</sup> or (2) CPT<sup>74</sup>. The type of therapy was chosen by the patient and the therapist. Importantly, all patients received psychotherapy in their participating Veterans Affairs PTSD clinic. Treatment outcome was assessed using the CAPS scale for DSM-IV and DSM-5.

**Resting-state EEG acquisition.** EEG data of the replication PTSD dataset were collected using an Electrical Geodesics (EGI) amplifier at sampling rate of 1 kHz with 256 saline-based electrodes. For both datasets, the electrode impedances were kept below 50 kΩ during the data recordings. During the experiment, participants were seated on a comfortable chair and instructed to remain awake and complete two sessions (ten-minute eyes-closed and ten-minute eyes-open paradigms).

**Resting-state EEG pre-processing.** The recorded rsEEG data were cleaned offline with the identical fully automated artefact rejection pipeline as used in PTSD study dataset 1.

**Resting-state fMRI acquisition.** Structural and functional MRI data were acquired on a 3T General Electrical scanner. The T1 structural MRI was scanned with parameters: BRAVO sequence acquired sagitally using an eight-channel coil, two-dimensional image reconstruction matrix of 256 × 256, flip angle 15°, slice thickness 1 mm, repetition time 8.208 ms, echo time 3.22 ms, field of view 24 cm. The functional MRI was scanned with parameters: a gradient echo epi simultaneous multislice sequence acquired axially using a 32-channel coil, two-dimensional image reconstruction matrix 70 × 70, slice thickness 4 mm, flip angle 45°, repetition time 700 ms, echo time 30 ms, field of view 22 cm. For rsfMRI, participants were instructed to keep their eyes open and fixated on a cross. Each ten-minute run yielded 851 fMRI volumes in each session.

**fMRI pre-processing.** The same pre-processing pipeline as used in PTSD study dataset 1 was adopted here for fMRI pre-processing.

**Depression study dataset 3. Trial registration.** Establishing Moderators and Biosignatures of Antidepressant Response for Clinical Care for Depression (EMBARC) is registered with ClinicalTrials.gov (identifier: NCT 01407094).

**Participants and treatment.** Written informed consent was obtained from each participant under institutional-review-board-approved protocols at each of

the four study sites: University of Texas Southwestern Medical Center (TX), Massachusetts General Hospital (MG), Columbia University (CU) and University of Michigan (UM). Data reported here are based on participants in the EMBARC study who were randomly assigned to sertraline or placebo during stage 1 of the trial ( $N=309$  total)<sup>75,76</sup>. Key eligibility for the study included the following: being 18–65 years old; having major depression as a primary diagnosis by the Structured Clinical Interview for DSM-IV Axis I Disorders (SCID) 1; at least moderate depression severity with a score ≥14 on the Quick Inventory of Depressive Symptomatology-Self Report (QIDS-SR) at screening and randomization; a major depressive episode beginning before age 30; either a chronic recurrent episode (duration ≥2 years) or recurrent MDD (at least two lifetime episodes); no antidepressant failure during the current episode. Exclusion criteria included the following: current pregnancy, breastfeeding, no use of contraception; lifetime history of psychosis or bipolar disorder; substance dependence in the past six months or substance abuse in the past two months; unstable psychiatric or general medical conditions requiring hospitalization; study medication contraindication; clinically significant laboratory abnormalities; history of epilepsy or condition requiring an anticonvulsant; electroconvulsive therapy, vagal nerve stimulation, TMS or other somatic treatments in the current episode; medications (including but not limited to antipsychotics and mood stabilizers); current psychotherapy; significant suicide risk; or failure to respond to any antidepressant at adequate dose and duration in the current episode.

EMBARC used a double-blind design, wherein participants were randomized to an eight-week course of sertraline or placebo (Supplementary Fig. 13). Randomization was stratified by site, depression severity and chronicity using a block randomization procedure. Sertraline dosing began at 50 mg using 50 mg capsules and was increased as tolerated if the patient did not respond until a maximum of 200 mg (ref. 75). A similar dosing approach was used for placebo capsules. Participant information is summarized in Supplementary Table 7. The primary outcome was the HAMD<sub>17</sub>. For participants lacking an endpoint HAMD<sub>17</sub>, multiple imputation by chained equations was conducted in R<sup>76</sup> using the package mice<sup>77</sup>. The following observed variables were utilized to impute endpoint HAMD<sub>17</sub> values for missing data via Bayesian regression: baseline HAMD<sub>17</sub>, week 1 HAMD<sub>17</sub>, week 2 HAMD<sub>17</sub>, week 3 HAMD<sub>17</sub>, week 4 HAMD<sub>17</sub>, week 6 HAMD<sub>17</sub>, baseline QIDS total score, baseline Mood and Symptom Questionnaire subscale scores for anxious arousal, anhedonic depression, and general distress, Snaith-Hamilton Pleasure Scale (SHAPS) total score, age, years of education, gender and Wechsler Abbreviated Scale of Intelligence (WASI) t-scores for vocabulary and matrix reasoning.

**Resting-state EEG acquisition.** rsEEG were recorded from each of the four study sites, including Columbia University, University of Texas Southwestern Medical Center, University of Michigan and Massachusetts General Hospital. At Columbia University, 72-channel EEG were collected using a 24-bit BioSemi system (sampling rate, 256 Hz; bandpass, DC–251.3 Hz), a Lycra stretch electrode cap (Electro-Cap International), and an active reference at electrode locations PPO1 and PPO2. At McLean Hospital, 129-channel EEG data were collected using a Geodesic Net system (sampling rate, 250 Hz; bandpass, 0.01–100 Hz), with Cz as reference (Electrical Geodesics). At the University of Michigan, 60-channel EEG data were collected using the 32-bit NeuroScan Synamp (Compumedics) system (sampling rate, 250 Hz; bandpass, 0.5–100 Hz), a Lycra stretch electrode cap and a nose reference. Finally, at the University of Texas Southwestern Medical Center, 62-channel EEG data were recorded (sampling rate, 250 Hz; bandpass, DC–100 Hz) using a 32-bit NeuroScan Synamp system, a Lycra stretch electrode cap and a nose reference. At all study sites, amplifier calibrations were performed. Experimenters were certified by the Columbia EEG team after demonstrating accurate EEG cap placement and delivery of task instructions via video conference, and then submitting satisfactory EEG data from a pilot subject. rsEEG were recorded during four two-minute blocks (two blocks for eyes closed and two blocks for eyes open) in a counterbalanced order. Participants were instructed to remain still and minimize blinks or eye movements, and to fixate on a centrally presented cross during the eyes-open condition.

**Resting-state EEG pre-processing.** The recorded rsEEG data were cleaned offline with the identical fully automated artefact rejection pipeline as used in PTSD study dataset 1. After artefact rejection, 54 EEG channels common to all four study sites were identified and extracted for each subject. Consequently, of the 266 patients with pre-treatment EEG recordings, 228 had usable EEG data for analyses. The 38 patients with unusable EEG recordings mainly had too many bad EEG channels and exceedingly large total power across channels.

**Resting-state fMRI acquisition.** Structural and functional MRI were collected using 3 tesla scanners from the four different sites. The rsfMRI data were acquired via T2<sup>\*</sup>-weighted images using single-shot gradient echo-planar imaging sequence during six minutes, comprising 180 volumes covering 39 axial slices with repetition time 2,000 ms, echo time 28 ms, flip angle 90°, matrix size 64 × 64, and voxel size 3.2 × 3.2 × 3.1 mm<sup>3</sup>. Participants were instructed to keep their eyes open during the scanning. T1-weighted structural three-dimensional axial images were acquired in the same session with parameters: Phillips scanner, series MPAGE, repetition

time 8 ms, echo time 3.7 ms, flip angle 12°, voxel size  $1 \times 1 \times 1 \text{ mm}^3$  for TX site; Siemens scanner, series MPAGE, repetition time 2.3 ms, echo time 2.54 ms, flip angle 9°, voxel size  $1 \times 1 \times 1 \text{ mm}^3$  for MG site; General Electrical scanner, series IR FSPGR, repetition time 6 ms, echo time 2.4 ms, flip angle 9°, voxel size  $1 \times 1 \times 1 \text{ mm}^3$  for CU site; Phillips scanner, series TFE, repetition time 8.1 ms, echo time 3.7 ms, flip angle 12°, voxel size  $1 \times 1 \times 1 \text{ mm}^3$  for UM site. More details of the acquisition parameters can be found in the literature<sup>9</sup>.

*fMRI pre-processing.* The same pre-processing pipeline as used in PTSD study dataset 1 was adopted here for fMRI pre-processing.

**Depression study dataset 4. Participants.** This dataset was based on a naturalistic open-label clinical study, and has been previously reported in detail elsewhere<sup>28,79</sup>. Briefly, 179 patients were drawn from three outpatient mental healthcare clinics in the Netherlands (neuroCare Clinic Nijmegen, neuroCare Clinic The Hague and Psychogenpraktijk Timmers Oosterhout) between May 2007 and November 2016. Inclusion criteria included: (1) a primary diagnosis of non-psychotic MDD or dysthymia, (2) BDI, second edition, Dutch version (BDI-II-NL)  $\geq 14$  at baseline, (3) treatment with at least ten sessions of rTMS over the DLPFC or early exit if response was achieved within ten sessions. All participants signed an informed consent. Additional exclusion criteria included: previous electroconvulsive therapy treatment, epilepsy, traumatic brain injury, current psychotic disorder, wearing a cardiac pacemaker or metal parts in the head and current pregnancy. The subject information is summarized in Supplementary Table 8.

*Resting-state EEG acquisition.* rsEEG data were acquired from 26 channels according to the 10–20 electrode international system (Quickcap; NuAmps). Data were referenced to averaged mastoids with a ground at AFz. The sampling rate of all channels was 500 Hz. A low-pass filter with attenuation of 40 dB per decade above 100 Hz was employed before digitization. Subjects were asked to rest quietly with their eyes open and eyes closed for 2 min each.

*Resting-state EEG pre-processing.* The recorded rsEEG data were cleaned offline with the identical fully automated artefact rejection pipeline as used in PTSD study dataset 1.

*Repetitive TMS treatment.* All patients were treated with either a high-frequency (10 Hz) protocol over the left DLPFC or a low-frequency (1 Hz) protocol over the right DLPFC, or both sequentially. The rTMS data included a long timespan, and the rTMS protocol applied was never based on clinical symptomatology. In the beginning (2006–2012) the standard protocol applied was 10 Hz left DLPFC rTMS, and only in some cases 1 Hz right DLPFC rTMS was applied (when there were concerns for safety, for example, paroxysmal activity, seizure risk) due to 1 Hz rTMS being considered a safer protocol. On first inspection of those data<sup>80</sup>, it was found that the clinical benefits for 10 Hz and 1 Hz were indistinguishable, after which time period the standard protocol became 1 Hz right DLPFC<sup>8</sup>. The analyses reported here focus only on patients that received only 10 Hz or 1 Hz rTMS as too few datasets were available on patients who received both treatments or switched treatments mid-way. There were 73 patients in the 10 Hz arm and 106 patients in the 1 Hz arm. Selection of the treatment protocol was not done in a randomized manner, but rather in the context of clinical care, and thus each arm is analysed separately. rTMS was performed using a Magstim Rapid2 (Magstim Company) or a Deymed DuoMag XT-100 stimulator with a figure-of-eight coil, 70 mm diameter. For the 10 Hz protocol, rTMS was administered at 10 Hz over the left DLPFC, 110–120% of the resting motor threshold, 30 trains of 5 s duration, inter-train interval 30 s, 1,500 pulses per session. The 1 Hz protocol consisted of rTMS at 1 Hz over the right DLPFC, 110–120% motor threshold, 120 trains of 10 s duration, inter-train interval 1 s, 1,200 pulses per session. The DLPFC was localized using either the 5 cm rule or the Beam F3/F4 method<sup>81</sup>. Furthermore, rTMS treatment was complemented with cognitive behavioural psychotherapy by a trained psychologist<sup>82</sup>. Psychotherapy was performed concurrent with the rTMS treatment in 45-minute sessions (the rTMS lasting 20 min). Sessions took place with a minimum frequency of two to three times per week and a maximum frequency of two per day, as per the patient's availability.

As these data were drawn from naturalistic clinical care, the total number of sessions depended on clinical decisions, and thus varied across patients. Decisions to continue treatment were based on response to treatment, clinical evaluation of symptom severity and the patient's own request. Decisions followed several rules: if a BDI decrease was observed of at least 20% from the baseline ten sessions, the treatment was continued, and re-evaluated every five sessions. If no response occurred by sessions 20–25, treatment was recommended to be terminated unless the patient requested to extend it. If BDI scores reached 12 or below for five sessions, which indicated remission, the patient was given the option of ending or tapering treatment, with an option to extend into maintenance sessions (one session every 6–8 weeks). However, if the threshold of BDI = 12 was reached, but symptom improvement continued, treatment was continued until BDI scores ceased improving.

*Clinical measurements.* Clinical outcome was assessed on the BDI (which was the primary outcome measure for the decision rules above) as well as the Depression,

Anxiety and Stress Scale (DASS)<sup>83</sup>. The DASS is a self-report questionnaire and consists of three subscales: depression (DASS-D), anxiety (DASS-A) and stress (DASS-S).

**Source-space PEC calculation.** In this study, we exploited the source-space PEC of EEG source signals as features for the subtyping analysis. PEC measures the correlation between the power envelopes of two band-limited spontaneous brain signals and therefore characterizes the amplitude synchrony between any pair of brain regions. By orthogonalizing the analytical time series of the two brain signals before calculating the power envelopes, PEC removes the zero-phase-lag connectivity, which is the primary source of spurious connectivity due to volume conduction<sup>36</sup>.

We first implemented source localization using the minimum-norm estimation approach<sup>84</sup> to convert the channel-space EEG into the source-space signals of 3,003 vertices. Specifically, a three-layer (scalp, skull and cortical surface) boundary element head model was computed with the OpenMEG plugin<sup>85</sup> based on FreeSurfer average brain template<sup>86</sup>. A total of 3,003 dipoles with unconstrained orientations were generated. The lead-field matrix relating the dipole activities to the EEG was obtained as a result of the boundary element modelling. Given channel-space EEG signals  $Z \in \mathbb{R}^{M \times T}$  of  $M$  channels and  $T$  sampling points and the lead-field matrix  $L \in \mathbb{R}^{M \times 9,009}$ , the source signals  $X \in \mathbb{R}^{9,009 \times T}$  could be estimated via

$$X = AZ \quad (1)$$

where  $A = RL^T(LRL^T + \lambda I)^{-1} \in \mathbb{R}^{9,009 \times M}$  is the inverse operator derived from the minimum-norm estimation.  $R \in \mathbb{R}^{9,009 \times 9,009}$  is the source covariance matrix encoding depth weights to compensate for the bias of assigning larger source estimates towards superficial locations,  $I \in \mathbb{R}^{M \times M}$  the noise covariance matrix and  $\lambda$  the regularization parameter. Following recommendations in the literature<sup>37,88</sup>,  $R = \text{diag}(r_i)$  with  $r_i = \left( \|L_{i,1}\|_2^2 + \|L_{i,2}\|_2^2 + \|L_{i,3}\|_2^2 \right)^{-1/2}$ , where  $L_{i,k}$  ( $k = 1, 2, 3$ ) are the three columns of  $L$  associated with the  $i$ th vertex,  $\lambda = \frac{\delta \times \text{trace}(\bar{L}\bar{L}^T)}{M}$ , where  $\bar{L} = I^{-1/2}L$  is the whitened lead-field matrix, and  $\delta$  is equal to the inverse of the power signal-to-noise ratio of the whitened EEG data  $\bar{Z} = I^{-1/2}Z$ . In our analysis,  $\delta = 1/81$ . For rsEEG, we assume the noises in different channels are uncorrelated and with equal variance. Hence, with the common average reference,  $\Gamma = (I_M - 1_M \times 1_M^T/M)(I_M - 1_M \times 1_M^T/M)^T$ , where  $I_M \in \mathbb{R}^{M \times M}$  is an identity matrix, and  $1_M \in \mathbb{R}^M$  an all-one vector.

Principal component analysis was next employed to reduce the three-dimensional estimated source signal at each vertex to the one-dimensional time series of the principal component. The analytical signal was then extracted at each vertex via the wavelet transform with the complex Morlet wavelet<sup>36</sup>. Consistent with the literature<sup>36</sup>, a spectral bandwidth of 0.5 octave ( $f/\sigma_f = 5.83$  and kernel size was  $6\sigma_f$ , with  $\sigma_f$  and  $\sigma_t$  being the spectral standard deviation and temporal standard deviation, respectively) was used for the wavelet transform. Subsequently, orthogonalization was carried out for the analytical signal of each vertex versus those of all other vertices to discount the spurious correlation resulting from the limited spatial resolution of source estimates, followed by computing their power envelopes<sup>36</sup>. Specifically, the orthogonalized component of an analytical signal  $Y(t)$  with respect to an analytical signal  $X(t)$  was defined at sampling point  $t$  as

$$Y_{\perp}(t) = \text{imag} \left( Y(t) \frac{X(t)^*}{|X(t)|} \right) \quad (2)$$

where  $X(t)^*$  denotes the conjugate of  $X(t)$ . The power envelopes were calculated as the square of the orthogonalized analytical signals, followed by a logarithmic transform to enhance normality. PEC was then calculated as the Pearson's correlation coefficient between the log-power envelopes at each pair of vertices, followed by the Fisher's  $r$ -to- $z$  transformation to enhance normality<sup>37,36</sup>.

The regional pairwise PEC features were further extracted among 31 cortical regions (Montreal Neurological Institute space) that were obtained from a parcellation of rsfMRI connectivity using independent component analysis applied to an independent set of subjects in a previous study<sup>27,89</sup>. For each pair of regions, connectivity was calculated by averaging PEC values over all possible vertex pairs. As a result, 465 unique regional pairwise connectivity features were computed in each of the four frequency bands and each of the two resting paradigms (eyes open and closed), followed by  $z$ -score normalization, and then used for the subsequent clustering-based subtyping analysis. The overall subtyping framework is illustrated in Supplementary Fig. 1.

To verify that the quality of the PEC estimates does not degrade when the vertex number decreases from 15,003 to 3,003, we compared the region of interest (ROI)-level PEC extracted with source localization between using 3,003 vertices and 15,003 vertices. PEC extracted based on 3,003 vertices is highly similar ( $r > 0.97$ ) to that based on 15,003 vertices (Supplementary Fig. 14a). In addition, we further compared the ROI-level mean PEC extracted using 3,003 vertices versus 15,003 vertices for all patients, subtype 1 and subtype 2, respectively. The results again show very high similarity ( $r > 0.99$ ) between using 3,003 vertices

and 15,003 vertices for all these cases (Supplementary Fig. 14b). All these results confirmed that using 3,003 vertices for source localization derived PEC that was very comparable to that of using 15,003 vertices. Therefore, we used 3,003 vertices for our study due to lower computational cost.

**Neurophysiological subtype identification.** For each participant, we combined PEC features extracted from all of the eight conditions to form a feature vector with dimensionality of  $465 \times 8 = 3,720$ . Such a large number of features typically include redundant information and the true underlying subtypes present in the data may differ only with respect to a portion of PEC features. To automatically determine the most distinct PEC features across all the conditions for more accurate identification of neurophysiological subtypes, we exploited a sparse K-means clustering algorithm<sup>29</sup> that provides an elegant way to achieve joint feature selection and clustering. Specifically, we define the between-cluster sum of squares for feature  $f$  as

$$\Omega_f = \left( \frac{1}{n} \sum_{i=1}^n \sum_{j=1}^n d_{i,j,f} - \sum_{k=1}^K \frac{1}{n_k} \sum_{i,j \in C_k} d_{i,j,f} \right) \quad (3)$$

where  $d_{i,j,f} = (x_{if} - \bar{x}_{jf})^2$  denotes the dissimilarity measure between observations  $i$  and  $j$  along feature  $f$ ,  $C_k$  consists of the indices of the observations in cluster  $k$ , and  $n_k$  is the number of observations in cluster  $k$ . The sparse K-means clustering is to find the solution to the following optimization problem:

$$\max_{C_1, \dots, C_K, w} \left\{ \sum_{f=1}^F w_f \Omega_f \right\}$$

$$\text{subject to } \|w\|^2 \leq 1, \|w\|_1 \leq s, w_f \geq 0 \forall f \quad (4)$$

where  $w \in \mathbb{R}^{3,720}$  is the weight vector to be estimated. Optimization problem (4) can be solved via an iterative algorithm<sup>29</sup>. As a result of the lasso-type sparsity constraint<sup>30</sup>  $\|w\|_1 \leq s$ , only the most important features have larger weights while zero weights are assigned to the majority of features. Thus, the sparse K-means clustering provides a data-driven approach for determining the potentially important connectivity biomarkers. In our analysis, an inner-loop cross-validation was carried out to determine the appropriate sparsity parameter  $s$  for feature selection. Based on the estimated sparse feature weights, K-means clustering was then implemented on the weighted feature subset to derive the optimal cluster solution, with the number of clusters determined by the gap statistic that compared the change in within-cluster dispersion with that expected under an appropriate reference null distribution<sup>31</sup>. The gap statistic chooses the cluster size based on one-standard-error criterion, finding the smallest value of  $k$  such that the gap value is within one standard deviation of the gap at  $k+1$ . In addition, variance ratio criterion (that is, the Calinski–Harabasz criterion<sup>32</sup>, defined as the ratio of between-cluster variance to within-cluster variance) was also used to assess the choice of the number of clusters.

**Clustering evaluation analysis.** The gap statistic indicated that two clusters yielded the best gap value satisfying the one-standard-error criterion (Supplementary Fig. 7a). The Calinski–Harabasz criterion further confirmed that two clusters achieved the maximum variance ratio and hence were the most distinct in the patient group (Supplementary Fig. 7b). To validate the stability of the identified subtypes, we repeatedly carried out clustering on multiple subsets of the whole samples. Specifically, we repeated the clustering analysis on 100 randomly selected subsamples (by leaving 10% of subjects out) of the dataset. For each subsample, subtype assignment stability was evaluated by testing whether pairs of subjects assigned to the same cluster had the same cluster labels obtained by clustering on the whole dataset. The stability performance was averaged over the 100 runs of clustering. The stability analysis confirmed that the two clusters also achieved the highest stability (Supplementary Fig. 7c,d). In addition, we also assessed the stability of cluster solution in dataset 1 across samples of healthy controls and compared it with that of patients. The subtyping stability of healthy controls (80.1%) was significantly lower (Wilcoxon rank sum statistical test:  $z=2.3, P=0.02$ ) than that of PTSD (91.9%) as well as more variable (coefficient of variation in healthy controls: 16.0, and in patients: 6.2) (Supplementary Fig. 9c).

**Pattern classification analysis.** To assess the transferability of our discovered subtypes across independent datasets, we implemented classification analysis by training a cluster-centroid-based classifier on one dataset (training set) and then applying it to another dataset (test set). Specifically, we performed sparse clustering on the training set to estimate the feature weights and derive the subtype labels. For each subtype, the cluster centroid was calculated from the weighted beta-band eyes-open PEC features belonging to the subtype. By applying the feature weights to the test set, we further calculated the Euclidean distance between the weighted test samples and each of the cluster centroids. A test sample was then classified as a subtype whose centroid has the smallest distance to the test sample. The classification accuracy was evaluated by comparing the predicted subtype labels

from the classifier with those obtained from clustering analysis of the test set. Similarly, we also adopted the same classification strategy to iteratively train the classifier on three datasets and tested on the fourth. In this case, the estimation of feature weights and identification of subtype labels were implemented on all three datasets in the training set instead of a single one.

**Subtype discriminability using rsfMRI.** To further validate that our identified subtypes indeed represent internally valid and neurobiologically meaningful phenotypes related to brain connectivity, we carried out a classification analysis to distinguish the two EEG-connectivity-driven subtypes using rsfMRI connectivity features. Specifically, regional pairwise fMRI connectivity was calculated using the same parcellation as that for EEG connectivity analysis. We pooled rsfMRI data (205 patients available for subtype 1 and 139 patients available for subtype 2) from scans acquired as part of datasets 1–3 for training a linear relevance vector machine<sup>92,93</sup> classifier. A  $10 \times 10$ -fold cross-validation was implemented to evaluate the classification performance including accuracy, sensitivity in detecting each subtype versus another and receiver operating characteristic curve. We regressed the effects of imaging site out of the fMRI data using multiple linear regression within the training set at each round of the cross-validation, and the residualized fMRI connectivity features were used for training the model. For each of ten repetitions, all subjects were randomly divided into ten folds, such that each subject was left out and used as a test set once while the remaining nine folds were used as training set for relevance vector machine model learning. The classification performance was then assessed over the ten repetitions. The significance of classification accuracy was further evaluated using 1,000 random label permutations.

**Reporting Summary.** Further information on research design is available in the Nature Research Reporting Summary linked to this article.

## Data availability

The data supporting the results in this study are available within the paper and its Supplementary Information. The dataset 3 (EMBARC data) is publicly available through the National Institute of Mental Health (NIMH) Data Archive ([https://ndar.nih.gov/edit\\_collection.html?id=2199](https://ndar.nih.gov/edit_collection.html?id=2199)). Access to the other datasets is governed by data-use agreements or sponsor restrictions, and they are therefore not publicly available.

## Code availability

The custom code used in this study is available for research purposes from the corresponding author on reasonable request.

Received: 18 September 2019; Accepted: 24 August 2020;

Published online: 19 October 2020

## References

- Kessler, R. C. et al. Lifetime prevalence and age-of-onset distributions of DSM-IV disorders in the National Comorbidity Survey Replication. *Arch. Gen. Psychiatry* **62**, 593–602 (2005).
- Belmaker, R. & Agam, G. Major depressive disorder. *N. Engl. J. Med.* **358**, 55–68 (2008).
- Hawco, C. et al. Separable and replicable neural strategies during social brain function in people with and without severe mental illness. *Am. J. Psychiatry* **176**, 521–530 (2019).
- Etkin, A. A reckoning and research agenda for neuroimaging in psychiatry. *Am. J. Psychiatry* **176**, 507–511 (2019).
- Etkin, A. Addressing the causality gap in human psychiatric neuroscience. *JAMA Psychiatry* **75**, 3–4 (2018).
- Etkin, A. & Wager, T. D. Functional neuroimaging of anxiety: a meta-analysis of emotional processing in PTSD, social anxiety disorder, and specific phobia. *Am. J. Psychiatry* **164**, 1476–1488 (2007).
- Wu, W. et al. An electroencephalographic signature predicts antidepressant response in major depression. *Nat. Biotechnol.* **38**, 439–447 (2020).
- Fonzo, G. et al. Brain regulation of emotional conflict predicts antidepressant treatment response for depression. *Nat. Hum. Behav.* **3**, 1319–1331 (2019).
- Chin Fatt, C. R. et al. Effect of intrinsic patterns of functional brain connectivity in moderating antidepressant treatment response in major depression. *Am. J. Psychiatry* **177**, 143–154 (2019).
- Berg, A. O. *Treatment of Posttraumatic Stress Disorder: An Assessment of The Evidence* (National Academies Press, 2008).
- Etkin, A. et al. Using fMRI connectivity to define a treatment-resistant form of post-traumatic stress disorder. *Sci. Transl. Med.* **11**, eaal3236 (2019).
- Wolfers, T. et al. Mapping the heterogeneous phenotype of schizophrenia and bipolar disorder using normative models. *JAMA Psychiatry* **75**, 1146–1155 (2018).
- Marquand, A. F. et al. Beyond lumping and splitting: a review of computational approaches for stratifying psychiatric disorders. *Biol. Psychiatry Cogn. Neurosci. Neuroimaging* **1**, 433–447 (2016).

14. Poulakis, K. et al. Heterogeneous patterns of brain atrophy in Alzheimer's disease. *Neurobiol. Aging* **65**, 98–108 (2018).
15. Orban, P. et al. Subtypes of functional brain connectivity as early markers of neurodegeneration in Alzheimer's disease. Preprint at <https://doi.org/10.1101/195164> (2017).
16. Wu, M.-J. et al. Identification and individualized prediction of clinical phenotypes in bipolar disorders using neurocognitive data, neuroimaging scans and machine learning. *NeuroImage* **145**, 254–264 (2017).
17. Karalunas, S. L. et al. Subtyping attention-deficit/hyperactivity disorder using temperament dimensions: toward biologically based nosologic criteria. *JAMA Psychiatry* **71**, 1015–1024 (2014).
18. Fonzo, G. A. et al. PTSD psychotherapy outcome predicted by brain activation during emotional reactivity and regulation. *Am. J. Psychiatry* **174**, 1163–1174 (2017).
19. Maron-Katz, A. et al. Individual patterns of abnormality in resting-state functional connectivity reveal two data-driven PTSD subgroups. *Am. J. Psychiatry* **177**, 244–253 (2020).
20. Palva, S. & Palva, J. M. Discovering oscillatory interaction networks with M/EEG: challenges and breakthroughs. *Trends Cogn. Sci.* **16**, 219–230 (2012).
21. Schoffelen, J. M. & Gross, J. Source connectivity analysis with MEG and EEG. *Hum. Brain Mapp.* **30**, 1857–1865 (2009).
22. He, B. et al. Electrophysiological brain connectivity: theory and implementation. *IEEE Trans. Biomed. Eng.* **66**, 2115–2137 (2019).
23. Brunner, C. et al. Volume conduction influences scalp-based connectivity estimates. *Front. Comput. Neurosci.* **10**, 121 (2016).
24. O'Neill, G. C. et al. Measuring electrophysiological connectivity by power envelope correlation: a technical review on MEG methods. *Phys. Med. Biol.* **60**, R271 (2015).
25. Brookes, M. J., Woolrich, M. W. & Barnes, G. R. Measuring functional connectivity in MEG: a multivariate approach insensitive to linear source leakage. *NeuroImage* **63**, 910–920 (2012).
26. Siems, M., Pape, A.-A., Hipp, J. F. & Siegel, M. Measuring the cortical correlation structure of spontaneous oscillatory activity with EEG and MEG. *NeuroImage* **129**, 345–355 (2016).
27. Toll, R. et al. An electroencephalography connectomic profile of post-traumatic stress disorder. *Am. J. Psychiatry* **177**, 233–243 (2020).
28. Colclough, G. L. et al. How reliable are MEG resting-state connectivity metrics? *NeuroImage* **138**, 284–293 (2016).
29. Witten, D. M. & Tibshirani, R. A framework for feature selection in clustering. *J. Am. Stat. Assoc.* **105**, 713–726 (2010).
30. Kass, R. E. & Raftery, A. Bayes factors. *J. Am. Stat. Assoc.* **90**, 773–795 (1995).
31. Tibshirani, R., Walther, G. & Hastie, T. Estimating the number of clusters in a data set via the gap statistic. *J. R. Stat. Soc. B* **63**, 411–423 (2001).
32. Price, R. B. et al. Parsing heterogeneity in the brain connectivity of depressed and healthy adults during positive mood. *Biol. Psychiatry* **81**, 347–357 (2017).
33. Lanius, R., Bluhm, R., Lanius, U. & Pain, C. A review of neuroimaging studies in PTSD: heterogeneity of response to symptom provocation. *J. Psychiatry Res.* **40**, 709–729 (2006).
34. Williams, L. M. et al. Childhood trauma predicts antidepressant response in adults with major depression: data from the randomized international study to predict optimized treatment for depression. *Transl. Psychiatry* **6**, e799 (2016).
35. Liston, C. et al. Default mode network mechanisms of transcranial magnetic stimulation in depression. *Biol. Psychiatry* **76**, 517–526 (2014).
36. Hipp, J. F. et al. Large-scale cortical correlation structure of spontaneous oscillatory activity. *Nat. Neurosci.* **15**, 884–890 (2012).
37. Brookes, M. J. et al. Investigating the electrophysiological basis of resting state networks using magnetoencephalography. *Proc. Natl Acad. Sci. USA* **108**, 16783–16788 (2011).
38. Mantini, D. et al. Electrophysiological signatures of resting state networks in the human brain. *Proc. Natl Acad. Sci. USA* **104**, 13170–13175 (2007).
39. Cabral, J. et al. Exploring mechanisms of spontaneous functional connectivity in MEG: how delayed network interactions lead to structured amplitude envelopes of band-pass filtered oscillations. *NeuroImage* **90**, 423–435 (2014).
40. Deco, G. et al. Single or multiple frequency generators in on-going brain activity: a mechanistic whole-brain model of empirical MEG data. *NeuroImage* **152**, 538–550 (2017).
41. Drysdale, A. T. et al. Resting-state connectivity biomarkers define neurophysiological subtypes of depression. *Nat. Med.* **23**, 28–38 (2017).
42. Dichter, G. S., Gibbs, D. & Smoski, M. J. A systematic review of relations between resting-state functional-MRI and treatment response in major depressive disorder. *J. Affect. Disord.* **172**, 8–17 (2015).
43. Klumpp, H. et al. Resting state amygdala-prefrontal connectivity predicts symptom change after cognitive behavioral therapy in generalized social anxiety disorder. *Biol. Mood Anxiety Disord.* **4**, 14 (2014).
44. Kumari, V. et al. Dorsolateral prefrontal cortex activity predicts responsiveness to cognitive-behavioral therapy in schizophrenia. *Biol. Psychiatry* **66**, 594–602 (2009).
45. Reggente, N. et al. Multivariate resting-state functional connectivity predicts response to cognitive behavioral therapy in obsessive-compulsive disorder. *Proc. Natl Acad. Sci. USA* **115**, 2222–2227 (2018).
46. Qin, J. et al. Predicting clinical responses in major depression using intrinsic functional connectivity. *NeuroReport* **26**, 675–680 (2015).
47. Goldstein-Piekarski, A. N. et al. Intrinsic functional connectivity predicts remission on antidepressants: a randomized controlled trial to identify clinically applicable imaging biomarkers. *Transl. Psychiatry* **8**, 57 (2018).
48. Spies, M. et al. Default mode network deactivation during emotion processing predicts early antidepressant response. *Transl. Psychiatry* **7**, e1008 (2017).
49. Wang, Q. et al. Identification of major depressive disorder and prediction of treatment response using functional connectivity between the prefrontal cortices and subgenual anterior cingulate: a real-world study. *J. Affect. Disord.* **252**, 365–372 (2019).
50. Olbrich, S. et al. Functional connectivity in major depression: increased phase synchronization between frontal cortical EEG-source estimates. *Psychiatry Res. Neuroimaging* **222**, 91–99 (2014).
51. George, M. S. et al. Daily repetitive transcranial magnetic stimulation (rTMS) improves mood in depression. *NeuroReport* **6**, 1853–1856 (1995).
52. Voigt, J., Carpenter, L. & Leuchter, A. Cost effectiveness analysis comparing repetitive transcranial magnetic stimulation to antidepressant medications after a first treatment failure for major depressive disorder in newly diagnosed patients—a lifetime analysis. *PLoS ONE* **12**, e0186950 (2017).
53. Nguyen, K.-H. & Gordon, L. G. Cost-effectiveness of repetitive transcranial magnetic stimulation versus antidepressant therapy for treatment-resistant depression. *Value Health* **18**, 597–604 (2015).
54. O'Reardon, J. P. et al. Efficacy and safety of transcranial magnetic stimulation in the acute treatment of major depression: a multisite randomized controlled trial. *Biol. Psychiatry* **62**, 1208–1216 (2007).
55. George, M. S. et al. Daily left prefrontal transcranial magnetic stimulation therapy for major depressive disorder: a sham-controlled randomized trial. *Arch. Gen. Psychiatry* **67**, 507–516 (2010).
56. Srinivasan, R., Tucker, D. M. & Murias, M. Estimating the spatial Nyquist of the human EEG. *Behav. Res. Meth. Instrum. Comput.* **30**, 8–19 (1998).
57. Palva, J. M. et al. Ghost interactions in MEG/EEG source space: a note of caution on inter-areal coupling measures. *NeuroImage* **173**, 632–643 (2018).
58. Olejarczyk, E., Marzetti, L., Pizzella, V. & Zappasodi, F. Comparison of connectivity analyses for resting state EEG data. *J. Neural Eng.* **14**, 036017 (2017).
59. Nolte, G. et al. Identifying true brain interaction from EEG data using the imaginary part of coherency. *Clin. Neurophysiol.* **115**, 2292–2307 (2004).
60. Vinck, M. et al. An improved index of phase-synchronization for electrophysiological data in the presence of volume-conduction, noise and sample-size bias. *NeuroImage* **55**, 1548–1565 (2011).
61. Geweke, J. F. Measures of conditional linear dependence and feedback between time series. *J. Am. Stat. Assoc.* **79**, 907–915 (1984).
62. Astolfi, L. et al. Estimation of the effective and functional human cortical connectivity with structural equation modeling and directed transfer function applied to high-resolution EEG. *Magn. Reson. Imaging* **22**, 1457–1470 (2004).
63. Astolfi, L. et al. Comparison of different cortical connectivity estimators for high-resolution EEG recordings. *Hum. Brain Mapp.* **28**, 143–157 (2007).
64. O'Neill, G. C. et al. Dynamics of large-scale electrophysiological networks: a technical review. *NeuroImage* **180**, 559–576 (2018).
65. Weathers, F. W. et al. The Clinician-Administered PTSD Scale for DSM-5 (CAPS-5): development and initial psychometric evaluation in military veterans. *Psychol. Assess.* **30**, 383–395 (2018).
66. First, M. B. in *The Encyclopedia of Clinical Psychology* (eds Cautin, R. L. & Lilienfeld, S. O.) 1–6 (Wiley, 2014).
67. Mullen, T. CleanLine: Tool/Resource Info (NeuroImaging Tools and Resources Collaboratory, 2012); <https://www.nitrc.org/projects/cleanline>
68. Perrin, F., Pernier, J., Bertrand, O. & Echallier, J. Spherical splines for scalp potential and current density mapping. *Electroencephalogr. Clin. Neurophysiol.* **72**, 184–187 (1989).
69. Bell, A. J. & Sejnowski, T. J. An information-maximization approach to blind separation and blind deconvolution. *Neural Comput.* **7**, 1129–1159 (1995).
70. Glover, G. H. et al. Function biomedical informatics research network recommendations for prospective multicenter functional MRI studies. *J. Magn. Reson. Imaging* **36**, 39–54 (2012).
71. Esteban, O. et al. fMRIprep: a robust preprocessing pipeline for functional MRI. *Nat. Methods* **16**, 111–116 (2019).
72. Jenkinson, M. et al. FSL. *NeuroImage* **62**, 782–790 (2012).
73. Foa, E. B. et al. A comparison of exposure therapy, stress inoculation training, and their combination for reducing posttraumatic stress disorder in female assault victims. *J. Consult. Clin. Psychol.* **67**, 194–200 (1999).
74. Resick, P. A. Cognitive therapy for posttraumatic stress disorder. *J. Cogn. Psychother.* **15**, 321–329 (2001).
75. Trivedi, M. H. et al. Establishing moderators and biosignatures of antidepressant response in clinical care (EMBARC): rationale and design. *J. Psychiatry Res.* **78**, 11–23 (2016).

76. R Core Team. R: A Language and Environment for Statistical Computing (R Foundation for Statistical Computing, 2013).
77. van Buuren, S. & Groothuis-Oudshoorn, K. Mice: multivariate imputation by chained equations in *R*. *J. Stat. Softw.* **45**, 1–67 (2011).
78. Donse, L. et al. Simultaneous rTMS and psychotherapy in major depressive disorder: clinical outcomes and predictors from a large naturalistic study. *Brain Stimul.* **11**, 337–345 (2018).
79. Krepl, N. et al. Non-replication of neurophysiological predictors of non-response to rTMS in depression and neurophysiological data-sharing proposal. *Brain Stimul.* **11**, 639–641 (2018).
80. Arns, M., Drinkenburg, W. H., Fitzgerald, P. B. & Kenemans, J. L. Neurophysiological predictors of non-response to rTMS in depression. *Brain Stimul.* **5**, 569–576 (2012).
81. Mir-Moghtadaei, A. et al. Concordance between BeamF3 and MRI-neuronavigated target sites for repetitive transcranial magnetic stimulation of the left dorsolateral prefrontal cortex. *Brain Stimul.* **8**, 965–973 (2015).
82. Beck, A. T. The current state of cognitive therapy: a 40-year retrospective. *Arch. Gen. Psychiatry* **62**, 953–959 (2005).
83. Lovibond, P. F. & Lovibond, S. H. The structure of negative emotional states: comparison of the Depression Anxiety Stress Scales (DASS) with the Beck Depression and Anxiety Inventories. *Behav. Res. Ther.* **33**, 335–343 (1995).
84. Hauk, O. Keep it simple: a case for using classical minimum norm estimation in the analysis of EEG and MEG data. *NeuroImage* **21**, 1612–1621 (2004).
85. Gramfort, A., Papadopoulou, T., Olivi, E. & Clerc, M. OpenMEEG: opensource software for quasistatic bioelectromagnetics. *Biomed. Eng. Online* **9**, 45 (2010).
86. Fischl, B. FreeSurfer. *NeuroImage* **62**, 774–781 (2012).
87. Hämäläinen, M. *MNE Software User's Guide* 59–75 (NMR Centre, Mass General Hospital, Harvard Univ., 2005).
88. Lin, F.-H. et al. Assessing and improving the spatial accuracy in MEG source localization by depth-weighted minimum-norm estimates. *NeuroImage* **31**, 160–171 (2006).
89. Chen, A. C. et al. Causal interactions between fronto-parietal central executive and default-mode networks in humans. *Proc. Natl Acad. Sci. USA* **110**, 19944–19949 (2013).
90. Tibshirani, R., Wainwright, M. & Hastie, T. *Statistical Learning with Sparsity: The Lasso and Generalizations* (Chapman and Hall/CRC, 2015).
91. Caliński, T. & Harabasz, J. A dendrite method for cluster analysis. *Commun. Stat. Theory Methods* **3**, 1–27 (1974).
92. Tipping, M. E. Sparse Bayesian learning and the relevance vector machine. *J. Mach. Learn. Res.* **1**, 211–244 (2001).
93. Zhu, H. et al. Multivariate classification of earthquake survivors with post-traumatic stress disorder based on large-scale brain networks. *Acta Psychiatr. Scand.* **141**, 285–298 (2020).

## Acknowledgements

This study was supported by grants from the Steven and Alexandra Cohen Foundation, Cohen Veterans Bioscience grant no. CVB034 and NIH grant nos. U01MH092221 and U01MH092250. A.E. was additionally funded by NIH grant no. DP1MH116506, and was previously supported by the Sierra-Pacific Mental Illness Research, Education and Clinical Center at the Veterans Affairs Palo Alto Healthcare System. Y.L. was supported by the Key R&D Program of Guangdong Province, China under grant no. 2018B030339001, National Key Research and Development Plan of China (no. 2017YFB1002505), and National Natural Science Foundation of China (no. 61633010). The support from N. Krepl in coordinating the TMS is acknowledged.

## Author contributions

Y.Z. contributed to the development of methods, analysis and interpretation of the data, and the drafting of the manuscript. W.W. contributed to the development of the methods, analysis and interpretation of the data and the drafting of the manuscript. R.T.T. contributed to the implementation of the connectivity calculation. S.N. contributed to the clinical data analysis. A.M.-K. and J.J. contributed to the fMRI data pre-processing. M.W., J.G., E.S., P.L., K.S., D.E.-S., C.C. and C.C.-F. contributed to the clinical and EEG collection. M.A. and M.S.G. oversaw the collection of clinical data. L.A. and Y.L. provided analytic input. M.H.T., C.R.M. and A.E. provided funding, oversaw the analysis and interpretation of the data, and drafting of the manuscript.

## Competing interests

A.E. receives equity and salary from Alto Neuroscience, along with equity from Mindstrong Health, Akili Interactive and Sizung. W.W. and J.G. receive equity and salary from Alto Neuroscience. C.R.M. receives equity from Receptor Life Sciences and consulting income from Otsuka Pharmaceuticals. The remaining authors declare no competing interests.

## Additional information

**Supplementary information** is available for this paper at <https://doi.org/10.1038/s41551-020-00614-8>.

**Correspondence and requests for materials** should be addressed to A.E.

**Reprints and permissions information** is available at [www.nature.com/reprints](http://www.nature.com/reprints).

**Publisher's note** Springer Nature remains neutral with regard to jurisdictional claims in published maps and institutional affiliations.

© The Author(s), under exclusive licence to Springer Nature Limited 2020

Corresponding author(s): Amit Etkin

Last updated by author(s): Jul 23, 2020

## Reporting Summary

Nature Research wishes to improve the reproducibility of the work that we publish. This form provides structure for consistency and transparency in reporting. For further information on Nature Research policies, see our [Editorial Policies](#) and the [Editorial Policy Checklist](#).

### Statistics

For all statistical analyses, confirm that the following items are present in the figure legend, table legend, main text, or Methods section.

n/a Confirmed

- The exact sample size ( $n$ ) for each experimental group/condition, given as a discrete number and unit of measurement
- A statement on whether measurements were taken from distinct samples or whether the same sample was measured repeatedly
- The statistical test(s) used AND whether they are one- or two-sided  
*Only common tests should be described solely by name; describe more complex techniques in the Methods section.*
- A description of all covariates tested
- A description of any assumptions or corrections, such as tests of normality and adjustment for multiple comparisons
- A full description of the statistical parameters including central tendency (e.g. means) or other basic estimates (e.g. regression coefficient) AND variation (e.g. standard deviation) or associated estimates of uncertainty (e.g. confidence intervals)
- For null hypothesis testing, the test statistic (e.g.  $F$ ,  $t$ ,  $r$ ) with confidence intervals, effect sizes, degrees of freedom and  $P$  value noted  
*Give P values as exact values whenever suitable.*
- For Bayesian analysis, information on the choice of priors and Markov chain Monte Carlo settings
- For hierarchical and complex designs, identification of the appropriate level for tests and full reporting of outcomes
- Estimates of effect sizes (e.g. Cohen's  $d$ , Pearson's  $r$ ), indicating how they were calculated

*Our web collection on [statistics for biologists](#) contains articles on many of the points above.*

### Software and code

Policy information about [availability of computer code](#)

Data collection	EEG data were collected by using the acquisition software provided with the EEG amplifiers. fMRI data were collected using scanners. Clinical and self-report data were collected by web and paper forms into the StudyTrax database.
Data analysis	EEG data were analyzed using the EEGLAB toolbox and custom Matlab code. fMRI data were preprocessed using fMRIprep pipeline and analysed using custom Matlab code.

For manuscripts utilizing custom algorithms or software that are central to the research but not yet described in published literature, software must be made available to editors and reviewers. We strongly encourage code deposition in a community repository (e.g. GitHub). See the Nature Research [guidelines for submitting code & software](#) for further information.

### Data

Policy information about [availability of data](#)

All manuscripts must include a [data availability statement](#). This statement should provide the following information, where applicable:

- Accession codes, unique identifiers, or web links for publicly available datasets
- A list of figures that have associated raw data
- A description of any restrictions on data availability

The data supporting the results in this study are available within the paper and its Supplementary Information. The dataset 3 (EMBARC data) is publicly available through the National Institute of Mental Health (NIMH) Data Archive ([https://nda.nih.gov/edit\\_collection.html?id=2199](https://nda.nih.gov/edit_collection.html?id=2199)). Access to the other datasets is governed by data-use agreements or sponsor restrictions, and they are therefore not publicly available.

# Field-specific reporting

Please select the one below that is the best fit for your research. If you are not sure, read the appropriate sections before making your selection.

Life sciences

Behavioural & social sciences

Ecological, evolutionary & environmental sciences

For a reference copy of the document with all sections, see [nature.com/documents/nr-reporting-summary-flat.pdf](https://nature.com/documents/nr-reporting-summary-flat.pdf)

## Life sciences study design

All studies must disclose on these points even when the disclosure is negative.

Sample size	PTSD Study Dataset 1: 106 patients and 95 healthy participants. PTSD Study Dataset 2: 135 patients. Depression Study Dataset 3: 266 patients. Depression Study Dataset 4: 179 patients.
Data exclusions	Subjects whose total powers across all the channels were beyond three standard deviations of the mean total power or having too many bad EEG channels were discarded.
Replication	The subtype findings were replicated using cross-validation across the four independent data sets.
Randomization	Depression study dataset 3: Patients were randomized 1:1 into the sertraline versus placebo treatment arms. Depression study dataset 4: Selection of the treatment protocol was not done in a randomized manner, but rather in the context of clinical care.
Blinding	For depression study dataset 3, all behavioral data acquisition occurred prior to randomization, and was thus blind to the treatment arm. Clinical assessors were also blind to the treatment arm.

## Reporting for specific materials, systems and methods

We require information from authors about some types of materials, experimental systems and methods used in many studies. Here, indicate whether each material, system or method listed is relevant to your study. If you are not sure if a list item applies to your research, read the appropriate section before selecting a response.

### Materials & experimental systems

n/a	Involved in the study
<input checked="" type="checkbox"/>	<input type="checkbox"/> Antibodies
<input checked="" type="checkbox"/>	<input type="checkbox"/> Eukaryotic cell lines
<input checked="" type="checkbox"/>	<input type="checkbox"/> Palaeontology and archaeology
<input checked="" type="checkbox"/>	<input type="checkbox"/> Animals and other organisms
<input type="checkbox"/>	<input checked="" type="checkbox"/> Human research participants
<input type="checkbox"/>	<input checked="" type="checkbox"/> Clinical data
<input type="checkbox"/>	<input type="checkbox"/> Dual use research of concern

### Methods

n/a	Involved in the study
<input checked="" type="checkbox"/>	<input type="checkbox"/> ChIP-seq
<input checked="" type="checkbox"/>	<input type="checkbox"/> Flow cytometry
<input type="checkbox"/>	<input checked="" type="checkbox"/> MRI-based neuroimaging

## Human research participants

Policy information about [studies involving human research participants](#)

### Population characteristics

The participant characteristics are presented here in brief.
For PTSD study dataset 1, all participants were combat veterans serving during the Operation Iraqi Freedom (Iraq), Operation Enduring Freedom (Afghanistan) and Operation New Dawn periods. Participants were recruited and assessed at either Stanford University or New York University after signing an informed consent approved by the relevant University's institutional review board, in accordance with the ethical principles in the Declaration of Helsinki. Psychiatric diagnoses, were based on DSM-V criteria using the Clinician-Administered PTSD Scale (CAPS), and for other diagnoses using the Structured Clinical Interview for DSM-IV (SCID). All diagnoses were confirmed in consensus clinician meetings. A history of traumatic brain injury (TBI) was determined based on whether loss of consciousness occurred after a combat-related head trauma.
For PTSD study dataset 2, all participants were recruited based on meeting clinical criteria for PTSD in the context of evaluation for psychotherapy treatment in a Veterans Affairs (VA) clinic located in either norther California or New Mexico. Written informed consent was obtained from each participant under institutional review board-approved protocol at Stanford University. All assessments occurred at Stanford, with participants recruited in New Mexico being flown, after signing a local written informed consent, to Stanford. Exclusion criteria followed those in dataset 1. Clinical severity was assessed using the CAPS interview for both DSM-IV and DSM-5, using self-reported BDI and WHOQOL.
For depression study dataset 3, written informed consent was obtained from each participant under institutional review board-approved protocols at each of the four clinical sites (University of Texas Southwestern Medical Center, Massachusetts General Hospital, Columbia University, and University of Michigan). Data reported here are based on EMBARC participants who were randomly assigned to sertraline or placebo during stage 1 of the trial (N=309 total). Key eligibility for the study

included being 18–65 years old, having major depression as a primary diagnosis by the Structured Clinical Interview for DSM-IV Axis I Disorders, at least moderate depression severity with a score ≥14 on the Quick Inventory of Depressive Symptomatology-Self Report (QIDS-SR) at screening and randomization, a major depressive episode beginning before age 30, either a chronic recurrent episode (duration ≥ 2 years) or recurrent MDD (at least 2 lifetime episodes), and no antidepressant failure during the current episode. Exclusion criteria included: current pregnancy, breastfeeding, no use of contraception; lifetime history of psychosis or bipolar disorder; substance dependence in the past six months or substance abuse in the past two months; unstable psychiatric or general medical conditions requiring hospitalization; study medication contraindication; clinically significant laboratory abnormalities; history of epilepsy or condition requiring an anticonvulsant; electroconvulsive therapy (ECT), vagal nerve stimulation (VNS), transcranial magnetic stimulation (TMS) or other somatic treatments in the current episode; medications (including but not limited to antipsychotics and mood stabilizers); current psychotherapy; significant suicide risk; or failure to respond to any antidepressant at adequate dose and duration in the current episode.

For depression study dataset 4, patients were drawn from three outpatient mental health care clinics in the Netherlands (neuroCare Clinic Nijmegen, neuroCare Clinic The Hague, and Psychogenpraktijk Timmers Oosterhout) between May 2007 and November 2016. Inclusion criteria included: 1) a primary diagnosis of non-psychotic MDD or dysthymia, 2) Beck Depression Inventory, second edition, Dutch version (BDI-II-NL)14 at baseline, 3) treatment with at least 10 sessions of rTMS over the DLPFC or response within these 10 sessions. All participants signed an informed consent under an approved IRB protocol. Additional exclusion criteria included: previous ECT treatment, epilepsy, traumatic brain injury, current psychotic disorder, wearing a cardiac pacemaker or metal parts in the head, and current pregnancy.

## Recruitment

See above

## Ethics oversight

The PTSD study dataset 1 was approved by Stanford University and New York University. The PTSD study dataset 2 was approved by Stanford University. The depression study dataset 3 was approved by each of the four study sites: University of Texas Southwestern Medical Center, Massachusetts General Hospital, Columbia University, and University of Michigan. The depression study dataset 4 was approved by neuroCare Clinic Nijmegen, neuroCare Clinic The Hague, and Psychogenpraktijk Timmers Oosterhout.

Note that full information on the approval of the study protocol must also be provided in the manuscript.

## Clinical data

### Policy information about [clinical studies](#)

All manuscripts should comply with the ICMJE [guidelines for publication of clinical research](#) and a completed [CONSORT checklist](#) must be included with all submissions.

#### Clinical trial registration

Establishing Moderators and Biosignatures of Antidepressant Response for Clinical Care for Depression (EMBARC), NCT#01407094

#### Study protocol

EMBARC used a double-blind design, wherein participants were randomized to an 8-week course of sertraline or placebo. Randomization was stratified by site, depression severity, and chronicity using a block randomization procedure. Sertraline dosing began at 50mg using 50mg capsules and was increased as tolerated if the patient did not respond until a maximum of 200mg 2. A similar dosing approach was used for placebo capsules.

#### Data collection

Data reported here are based on EMBARC participants who were randomly assigned to sertraline or placebo during stage 1 of the trial (N=309 total). Resting-state EEG (rsEEG) were recorded from each of the four study sites: University of Texas Southwestern Medical Center (TX), Massachusetts General Hospital (MG), Columbia University (CU), and University of Michigan (UM). At all study sites, amplifier calibrations were performed. Experimenters were certified by the Columbia EEG team after demonstrating accurate EEG cap placement and delivery of task instructions via video conference, and then submitting satisfactory EEG data from a pilot subject.

rsEEG were recorded during four 2-minute blocks (2 blocks for eyes-closed, and 2 blocks for eyes open) in a counterbalanced order. Participants were instructed to remain still and minimize blinks or eye movements, and to fixate on a centrally presented cross during the eyes-open condition.

Structural and functional MRI were collected using 3 Tesla scanners from the four different sites. The rsfMRI data were acquired via T2\*-weighted images using single-shot gradient echo-planar imaging sequence during 6-minute, comprising 180 volumes covering 39 axial slices with repetition time = 2000 ms, echo time = 28 ms, flip angle = 90 degrees, matrix size = 64×64, and voxel size = 3.2×3.2×3.1 mm<sup>3</sup>. T1-weighted structural 3D axial images were acquired in the same session with parameters: Phillips scanner, Series = MPAGE, repetition time = 8 ms, echo time = 3.7 ms, flip angle = 12 degrees, voxel size = 1×1×1 mm<sup>3</sup> for TX site; Siemens scanner, Series = MPAGE, repetition time = 2.3 ms, echo time = 2.54 ms, flip angle = 9 degrees, voxel size = 1×1×1 mm<sup>3</sup> for MG site; General Electrical scanner, Series = IR FSPGR, repetition time = 6 ms, echo time = 2.4 ms, flip angle = 9 degrees, voxel size = 1×1×1 mm<sup>3</sup> for CU site; Phillips scanner, Series = TFE, repetition time = 8.1 ms, echo time = 3.7 ms, flip angle = 12 degrees, voxel size = 1×1×1 mm<sup>3</sup> for UM site.

#### Outcomes

Our primary outcome was the Hamilton Depression Rating Scale (HAMD17). For participants lacking an endpoint HAMD17, multiple imputation by chained equations was conducted in R3 using the package mice 4. The following observed variables were utilized in order to impute endpoint HAMD17 values for missing data via Bayesian regression: baseline HAMD17, week 1 HAMD17, week 2 HAMD17, week 3 HAMD17, week 4 HAMD17, week 6 HAMD17, baseline Quick Inventory of Depressive Symptoms (QIDS) total score, baseline Mood and Symptom Questionnaire subscale scores for Anxious Arousal, Anhedonic Depression, and General Distress, Snaith-Hamilton Pleasure Scale (SHAPS) total score, age, years of education, gender, and Wechsler Abbreviated Scale of Intelligence (WASI) t-scores for Vocabulary and Matrix Reasoning.

# Magnetic resonance imaging

## Experimental design

Design type	Resting-state fMRI
Design specifications	N/A
Behavioral performance measures	N/A

## Acquisition

Imaging type(s)	Functional
Field strength	3 Tesla
Sequence & imaging parameters	<p>Dataset 1: rsfMRI was collected from each participant for eight minutes. Participants were scanned using either a GE 750 scanner at Stanford University or a Siemens 3T Skyra scanner at New York University. Both sites acquired 32 axial slices with 3.5 mm thickness using an echo-planar gradient-epoch T2-weighted pulse sequence (with 2000 ms repetition time; 29 ms echo time; 90 degrees flip angle; 0 slice spacing; 20 cm field of view; 64 x 64 matrix size). A high-resolution T1-weighted structural scan was acquired using three-dimensional MPRAGE in the sagittal plane with parameters: inversion time = 450 ms, TR = 8.21 ms, TE = 3.22 ms, flip angle = 15 degrees, field of view = 24 cm, 184 slices, matrix = 256 x 256, acquired resolution = 0.9375 x 0.9375 x 1.0 mm<sup>3</sup>.</p> <p>Dataset 2: rsfMRI data was acquired on a 3T GE scanner. The T1 structural MRI was scanned with parameters: BRAVO sequence acquired sagitally using a 8-channel coil, 2D image reconstruction matrix of 256 x 256, flip angle = 15 degrees, slice thickness = 1 mm, repetition time = 8.208 ms, echo time = 3.22 ms, field of view = 24 cm. The functional MRI was scanned with parameters: a gradient echo epi simultaneous multi-slice sequence acquired axially using a 32-channel coil, 2D image reconstruction matrix 70 x 70, slice thickness = 4 mm, flip angle = 45 degrees, repetition time = 700 ms, echo time = 30 ms, field of view = 22 cm. For rsfMRI, participants were instructed to keep their eyes open and fixated on a cross. Each 10-minute run yielded 851 fMRI volumes in each session.</p> <p>Dataset 3: Structural and functional MRI were collected using 3 Tesla scanners from the four different sites. The rsfMRI data were acquired via T2*-weighted images using single-shot gradient echo-planar imaging sequence during 6-minute, comprising 180 volumes covering 39 axial slices with repetition time = 2000 ms, echo time = 28 ms, flip angle = 90 degrees, matrix size = 64x64, and voxel size = 3.2x3.2x3.1 mm<sup>3</sup>. T1-weighted structural 3D axial images were acquired in the same session with parameters: Phillips scanner, Series = MPRAGE, repetition time = 8 ms, echo time = 3.7 ms, flip angle = 12 degrees, voxel size = 1x1x1 mm<sup>3</sup> for TX site; Siemens scanner, Series = MPRAGE, repetition time = 2.3 ms, echo time = 2.54 ms, flip angle = 9 degrees, voxel size = 1x1x1 mm<sup>3</sup> for MG site; General Electrical scanner, Series = IR FSPGR, repetition time = 6 ms, echo time = 2.4 ms, flip angle = 9 degrees, voxel size = 1x1x1 mm<sup>3</sup> for CU site; Phillips scanner, Series = TFE, repetition time = 8.1 ms, echo time = 3.7 ms, flip angle = 12 degrees, voxel size = 1x1x1 mm<sup>3</sup> for UM site.</p>

Area of acquisition	Whole brain
Diffusion MRI	<input type="checkbox"/> Used <input checked="" type="checkbox"/> Not used

## Preprocessing

Preprocessing software	fMRIprep pipeline
Normalization	Volume-based spatial normalization was performed through nonlinear registration using brain-extracted versions of both the T1-weighted image and template.
Normalization template	MNI152
Noise and artifact removal	Automatic removal of motion artifacts using ICA was performed on the preprocessed BOLD on MNI space time-series after removal of non-steady state volumes and spatial smoothing with an isotropic, Gaussian kernel of 6 mm full-width half-maximum.
Volume censoring	N/A

## Statistical modeling & inference

Model type and settings	Multivariate analysis based on relevance vector machine.
Effect(s) tested	N/A
Specify type of analysis:	<input type="checkbox"/> Whole brain <input checked="" type="checkbox"/> ROI-based <input type="checkbox"/> Both

Anatomical location(s)	The same parcellation as for EEG connectivity analysis was used for rsfMRI regional connectivity calculation.
Statistic type for inference (See <a href="#">Eklund et al. 2016</a> )	Multivariate classification analysis with ROI-level connectivity
Correction	N/A

## Models & analysis

n/a Involved in the study

Functional and/or effective connectivity

Graph analysis

Multivariate modeling or predictive analysis

Functional and/or effective connectivity

Pearson correlation

Multivariate modeling and predictive analysis

In order to further validate that our identified subtypes indeed represent internally valid and neurobiologically meaningful phenotypes related to brain connectivity, we carried out a classification analysis to distinguish the two EEG-connectivity driven subtypes using resting-state fMRI (rsfMRI) connectivity features. Specifically, regional pairwise fMRI connectivity was calculated using the same parcellation as that for EEG connectivity analysis. We pooled rsfMRI data (205 patients available for subtype 1 and 139 patients available for subtype 2) from scans acquired as part of datasets 1–3 for training a linear relevance vector machine (RVM) classifier. A 10x10-fold cross-validation was implemented to evaluate the classification performance including accuracy, sensitivity in detecting each subtype versus another, and ROC curve. We regressed the effects of imaging site out of the fMRI data using multiple linear regression within the training set at each round of the cross-validation, and the residualized fMRI connectivity features were used for training the model. For each of 10 repetitions, all subjects were randomly divided into 10 folds, such that each subject was left out and used as a test set once while the remaining nine folds were used as training set for RVM model learning. The classification performance was then assessed over the 10 repetitions. The significance of classification accuracy was further evaluated using 1,000 random label permutations.